Thermodynamic analysis of supercritical water gasification combined with a reversible solid oxide cell

Recalde, Mayra; Amladi, Amogh; Venkataraman, Vikrant; Woudstra, Theo; Aravind, Purushothaman Vellayani

DOI
10.1016/j.enconman.2022.116208

Publication date
2022

Document Version
Final published version

Published in
Energy Conversion and Management

Energy Conversion and Management 270 (2022) 116208

Contents lists available at ScienceDirect

Energy Conversion and Management

journal homepage: www.elsevier.com/locate/enconman

Thermodynamic analysis of supercritical water gasification combined with a reversible solid oxide cell

Mayra Recalde [a,*], Amogh Amladi [b], Vikrant Venkataraman [c], Theo Woudstra [a,b], Purushothaman Vellayani Aravind [a,b]

[a] Process & Energy, 3me Delft University of Technology, Leeghwaterstraat 39, 2628 CA Delft, the Netherlands
[b] Energy and Sustainability Research Institute Groningen, Faculty of Science and Engineering, University of Groningen, Nijenborgh 6, 9747 AG Groningen, the Netherlands
[c] Fuel Cell Business Unit, Instrumentation and Test Systems, AVL List GmbH, Hans List Platz 1, 8020 Graz, Austria

ARTICLE INFO

Keywords:
Supercritical water gasification
Reversible solid-oxide cell
Biomass
Syngas
Renewable energy
Aspen Plus

ABSTRACT

The low cost of electricity in some areas facilitates the adoption of high-temperature electrolysis plants for the large-scale storage of electricity. Supercritical water gasification (SCWG) is a promising method of syngas production from wet biomass. Additionally, it is a potential source of steam for electrochemical plants. However, the commercialisation of standalone SCWG systems is hindered by low efficiency and high operating cost. Accordingly, we propose the integration of SCWG with a reversible solid oxide cell (rSOC) to realise simultaneous syngas or power generation and wet biomass conversion. This technique would make the process feasible in terms of energy, allowing engineers to use SCWG to combine power generation with fuel production. The wet syngas from the SCWG is fed to the rSOC powered by excess renewable electricity in electrolysis mode, where steam is reduced to H_2 to produce dry syngas with a higher calorific value. The energy efficiency of the proposed system is 91% in electrolysis mode and 47% in fuel cell mode. The electrolysis increases the syngas yield by a factor of thirteen and the use of total syngas generates twelve times more power in fuel cell mode compared to the use of only fresh syngas from SCWG.

1. Introduction

Solutions to combat climate change and to improve sanitation infrastructure globally are fundamental for sustainable development of society. According to previous studies [1] renewable energy will constitute 14 % of global energy sources worldwide by 2040 under current policies for a faster-growing energy source than oil or natural gas [2]. As a result, the price of renewable electricity is falling globally and is already quite low in some areas; for example, it is 13.5 USD MWh^{-1} in the United Arab Emirates [3]. However, renewable energy sources such as wind and solar are intermittent. Therefore, there is a need for development of efficient energy storage solutions.

Wet organic matter such as manure, sewage, and industrial waste is currently the most significant source of global water pollution [4]. Sanitation-related diseases cause approximately 2.2 million deaths per year (mostly children younger than five) [5]. Therefore, conversion of wet organic matter (wet biomass) into biofuel will not only provide health and environmental benefits, but also provide a valuable source of sustainable energy.

A high-temperature electrolysis process utilises electricity and heat to produce hydrogen (or syngas) from steam and CO_2, which can be used directly as a fuel, or raw material for production of other synthetic fuels. Any process that generates a high concentration of steam or CO_2 is a potential source of these reactants for electrolysis. The electricity and heat required for the electrochemical reaction may come from sources such as solar, wind, industrial process waste heat, geothermal, or nuclear energy.

Solid oxide fuel cells (SOFC) are high efficiency devices used to produce electricity directly from fuels by electrochemical oxidation, without NOx production. For stationary power generation, SOFC-GT (gas turbine) combined cycles are the systems with the highest efficiency [6]. At present, SOFC technology has reached high TRL (Technological Readiness Level) levels (8 or above), prompting various companies to offer SOFC products, Solid Power, Sunfire, etc. [7].

A combination of SOEC and SOFC systems can be used to convert renewable electricity to synthetic fuels, and later utilise these fuels to produce electricity again; thus, acting like a renewable energy storage

* Corresponding author.
E-mail address: m.recaldem@outlook.com (M. Recalde).

https://doi.org/10.1016/j.enconman.2022.116208
Received 25 March 2022; Received in revised form 12 August 2022; Accepted 3 September 2022
Available online 12 September 2022

Nomenclature

A	area of the stack (cm^2)
d_p	particle diameter (nm)
E	cell voltage (V)
E_r	reversible potential (V)
e_f	specific flow exergy per unit of mol (kJ mol^{-1})
Ex	exergy (kW)
$\overline{ex}_i^{ch}$	chemical exergy (kJ mol^{-1})
$\dot{E}_d$	exergy destruction rate (kW)
F	Faraday constant (C mol^{-1})
ΔG	change in specific molar Gibbs free energy ($Jmol^{-1}$)
ΔH	change in specific molar enthalpy ($Jmol^{-1}$)
h	specific enthalpy (kJ kg^{-1})
I	current (A)
j	current density (Acm^{-2})
$\dot{m}$	mass flow rate (kg s^{-1})
M	molecular weight (g mol^{-1})
n	number of moles
$\dot{n}$	mole flow rate (mol s^{-1})
P	pressure (Pa), power (kW),
p	partial pressure
Q	heat (kW)
R	gas constant ($Jmol^{-1}K^{-1}$)
ΔS	change in specific molar entropy (kJ mol K^{-1})
S	specific entropy (kJ K kg^{-1})
T	temperature (K)
U_f	fuel utilisation ratio
V	voltage (V)
x	mass fraction
y	mole fraction
$\dot{W}$	rate of work (kW)

Greek letters

Δ	thickness (μm)
β	surface ratio
η	efficiency, cell resistant (Ω m^2)
τ	tortuosity
ε	porosity
μ	chemical potential ($Jmol^{-1}$)
Γ	surface site density (mol cm^2)
δ	conductivity

Subscripts, superscript

act	activation
ch	chemical
conc	concentration
cv	control volumen
des	desorption
e	exit
f	thermochemical
ex	exergy
i	inlet, mixture components
j	number of component present in a mixture
0	properties at the reference environment
ohm	Ohmic
ox	oxidant
r	reversible
sys	system
TN	thermoneutral
an	anode
cat	cathode

Abbreviations

BOP	balance of the plant
CGE	cold gas efficiency
CE	carbon gasification efficiency
SCWG	supercritical water gasification
GT	gas turbine
GUP	gas upgrading unit
LHV	lower heating value ($kJmol^{-1}$)
HE	heat exchanger
HHV	high heating value ($kJmol^{-1}$)
PSC	post combustor
TPB	three-phase boundary
ASR	area-specific resistance
rSOC	reversible-solid oxide cell
SOFC	solid-oxide fuel cell
SOEC	solid-oxide electrolyser cell
SEP	gas/liquid separator
SCW	supercritical water

system. In the recent years, there has been increasing research on the concept of reversible solid oxide cells (rSOC). The main advantage of this concept is that the same SOC device can operate both in fuel cell (FC) and electrolysis (EL) mode, and in some cases, the same balance-of-plant (BOP) component can also be used in both modes. This reduces the capital cost of such a renewable energy storage system, while retaining the high efficiency benefits of SOC systems.

Some researchers have studied the integration of biomass gasification with SOEC systems. Sigurjonsson et al. [8] investigated the integration of rSOC with biomass gasification for hydrogen or power generation. The system reaches an efficiency of 46 % for fuel production from biomass with a moisture content of 45 wt%. Clausen et al. [9] examined the combined gasifier and pressurized SOEC system. The energy efficiency achieved was 84 % for syngas production from wood pellets. In another research, Anghilante [10] proposed the upgrading of bio-syngas through steam electrolysis and catalytic methanation achieving an energy efficiency in the range of 78.5–81.8 %. Ali et al. [11] investigated straw biomass gasification and SOEC combined system for methanol production. The system reaches an energy efficiency of 72.08 %, at a biomass moisture content of 7.9 wt%. Yi et al. [12] analysed and optimized a biomass-fuelled polygeneration system for electricity, hydrogen, and freshwater generation. The system combined a Rankine cycle, a multi-effect desalination, and a solid oxide electrolyser and achieved a total exergy efficiency of 17.64 %. Habibollahzade et al. [13] analysed and optimized the integrated hybrid biomass-based solid oxide fuel cell/solid oxide electrolyser cell/gas turbine using different gasification agents. The system achieves an exergy efficiency of 45.25 % for power and hydrogen production. For the systems mentioned above it is difficult to compare the efficiencies since for poly-generation systems the definition of efficiency requires a different approach.

According to the literature review, the integration of gasification technology with SOEC technology combines the advantages of the two. Heat integration improves thermal performance. The oxygen by-product of electrolysis acts as a gasifying agent. Therefore, the fuel is produced with high energy efficiency > 70 % [9,10,11]. However, the efficiency of fuel and power production in the poly-generation system reduces to $<$ 50 % [12,13]. There is a lack of studies on highly efficient fuel and/or power generation using wet biomass feedstock. The integrated systems analysed are limited to conventional biomass with a moisture content lower than 10 wt%. Higher moisture in biomass requires an energy demanding dryer unit, reducing the efficiency of the systems. It is reflected in the efficiency of 46 % found in the work of Sigurjonsson et al.

Table 1
Fuel and power SCWG combined system.

Integrated System	P bar	T ° C	con. wt.%	η %	η_{ex} %	Prod.	Ref.
SCWG–SOFC-GT	250	600	21.52	50	50	Power	[35]
Hydrothermal gasification-Catalytic fixed-bed gasific SOFC-RNK-FP-GT	300	350–450	20	63	60	Power	[36]
SCWG-direct expansion in a gas supercritical turbine- combined cycle.	250	650	25	54.38		Power	[37]
Solar SCWG – SMR	240	605	25	45	45	syngas	[28]
SCWG-syngas chemical looping (SCL)-power generation		650	15	73		Power + H_2	[32]
Solar SCWG – SMR	240–250	590–605	13–15.4	81.26	50.31	syngas	[26]
SCWG – syngas separation Rankine cycle	250	650	20 8		89.18 20	Power + syngas	[31]

[8].

SCWG is a process that converts wet biomass into combustibles with useful minerals as by-products [14]. A separation system can easily recover the minerals contained in the biomass, given that minerals have low solubility in water at supercritical conditions. A gas cleaning unit at temperature > 374 °C, and pressure > 221 bar recovers the salt [15,16]. The addition of a ZnO bed in the SCWG reactor enables sulphur removal [17 18]. Hence, the product gas is relatively clean to feed a SOC without causing degradation of the SOC anode. This process operates at relatively low temperatures between 400 °C and 600 °C and pressures above 220 bar. The variation of thermo-physical properties of supercritical water (SCW) significantly influences the heat transfer and the biomass gasification [19,20]. The main advantage of SCWG is that it does not need an energy-intensive biomass-drying step since it uses water as both the reactant and the reaction medium.

The SCWG technique is still not widely commercialised and needs some research and development because it is hindered by high operating costs and multiple engineering challenges. Nearly 100 % conversion of biomass (minimization of char formation) into syngas requires high temperatures (>600 °C without catalyst), feasible residence time and low feedstock concentration [21,22,23]. The thermodynamic efficiency is affected by high energy requirements, which requires a heat recovery system [22]. The resulting gas contains high concentration of steam and CO_2. Chen et al. [24] suggested increasing the system capacity, feedstock concentration, improving the heat transfer efficiency and energy recovery, etc. to contribute to the reduction in hydrogen production cost and the improvement in the thermodynamic efficiency.

Table 1 shows the operating conditions and performance of several integrated SCWG systems for fuel and/or power production. The energy efficiency reached by these systems is in the range of 50 to 82 %. The feedstock concentration is between 13 % and 25 %. Thermal efficiency and CGE (cold gas efficiency) are favoured at feedstock concentrations > 10 wt% [25,26] because of the higher CO and CH_4 content in the syngas [27]. But the exergy efficiency decayed due to increased char formation [28,26]. In this regard, high feedstock concentration harms the gasification, since water influences the physics and chemistry that determines supercritical water gasification [29,30]. It is demonstrated nearly complete gasification of 99.2 % CE (carbon gasification efficiency) at feedstock concentration of 9 wt% chicken manure at 620 °C [25]. On the contrary, the high moisture content leads to a high energy requirement for increasing the temperature to supercritical conditions, substantially reducing the exergy efficiency. Chen et al. [31] reported a decrease in the SCWG exergy efficiency from ~ 90 % at 20 wt% biomass to ~ 20 % at 8 wt% biomass. Thus, a trade-off between complete gasification and thermal efficiency is required.

The SCWG product gas, with high exergy, contains a high amount of steam, which is usually condensed out (gas upgrading unit) before utilisation of the gas as fuel. The systems indicated in Table 1 recover the exergy of the product gas, before entering a gas upgrading unit, with a HE (heat exchanger) or with chemical looping (oxy-fuel combustion using a solid-state oxygen carrier). These units recover the sensible heat of the product gas to recirculate in the process. Ajiwibowo et al. [32] uses chemical looping in co-production of H_2 and recovers the heat for power generation. The system reaches an energy efficiency of 73 %. Chen et al. [31] uses a HE for heat recovery and power generation. The HE recovers most of the sensible heat of the gasification product gas. The heat recovered pre-heats the water entering the SCWG and heats the water that feeds a Rankine cycle. The system reaches an exergy efficiency of 89.18 % at 20 wt% biomass (80 wt% water) but reduces to 20 % at 8 wt% biomass. The exergy destruction of the energy recovery units accounts for a significant fraction of the total exergy destruction in the system [31,26]. Guo et al. [33] presented direct mass transfer system as an alternative to the HE. The highest exergy efficiency, around 90 %, is reached at feedstock concentration of 70.6 wt% biomass; at 30 wt% biomass the efficiency reduces to 30 % approximately. In addition, the oxygen demand by the system will imply additional operation costs.

The gas upgrading unit negatively influences the overall system efficiency. It depends on the high-water content and the inlet gas-product temperature. High inlet temperature of the gas upgrading unit results in high waste heat production in the system [28,34]. The syngas obtained after the condensation still contains a high volume of CO_2 (22 vol%, SCWG operating at 420 °C, 280 bar) [18], which reduces its calorific value. Onigbajumo et al. [26] fed the product gas to a reforming reactor promoting, simultaneously, the water gas shift reaction. However, the reactors represent 60 % of the total exergy destruction of the process [26] and [28]. The higher the system complexity the higher exergy destruction. It is reflected in the exergy efficiency of 50.31 % in the work of Onigbajumo.

From this perspective, feedstock concentration lower than 10 wt% can be an alternative to address the char formation issue, achieving a high conversion of feedstock in SCWG, despite the high energy demand to increase the temperature to supercritical conditions. Process integration makes heat recovery feasible and reduction of exergy destruction in HE, gas–liquid separation unit and reforming reactors, by applying simpler system configuration. In this context, the gasifier product gas (salt separation in the gas cleaning unit Temperature > 374 °C, Pressure > 221 bar [15,16]), when excess renewable electricity is available, can be directly fed to an rSOC in EL mode. The fuel electrode promotes the electrochemical reduction of H_2O into H_2 and O_2. It increases the exergy of the produced gas and thus the capacity of the system. SOEC anode is able to support electrolysis. Additionally, it also supports water–gas shift reaction and methanation reaction (the latter at pressurised operation [38]).

The combustible gas and the air-based streams release heat during the downstream cooling process. This provides the energy required to pre-heat the feedstock to supercritical conditions. Heat is also provided for SOEC air preheating. The water content of the product syngas is significantly reduced thanks to electrolysis. The high-value syngas generated can be stored for later use in the rSOC in FC mode. When there is a deficit of renewable electricity, the stored syngas is mixed with the fresh syngas from the SCWG system (after gas upgrading), and used in the rSOC in FC mode to generate electricity.

The objective of this study is to develop a process design for a combined SCWG-rSOC system that significantly increases the system capacity for hydrogen production, which could reduce operating costs and achieve high thermodynamic efficiency by reducing exergy

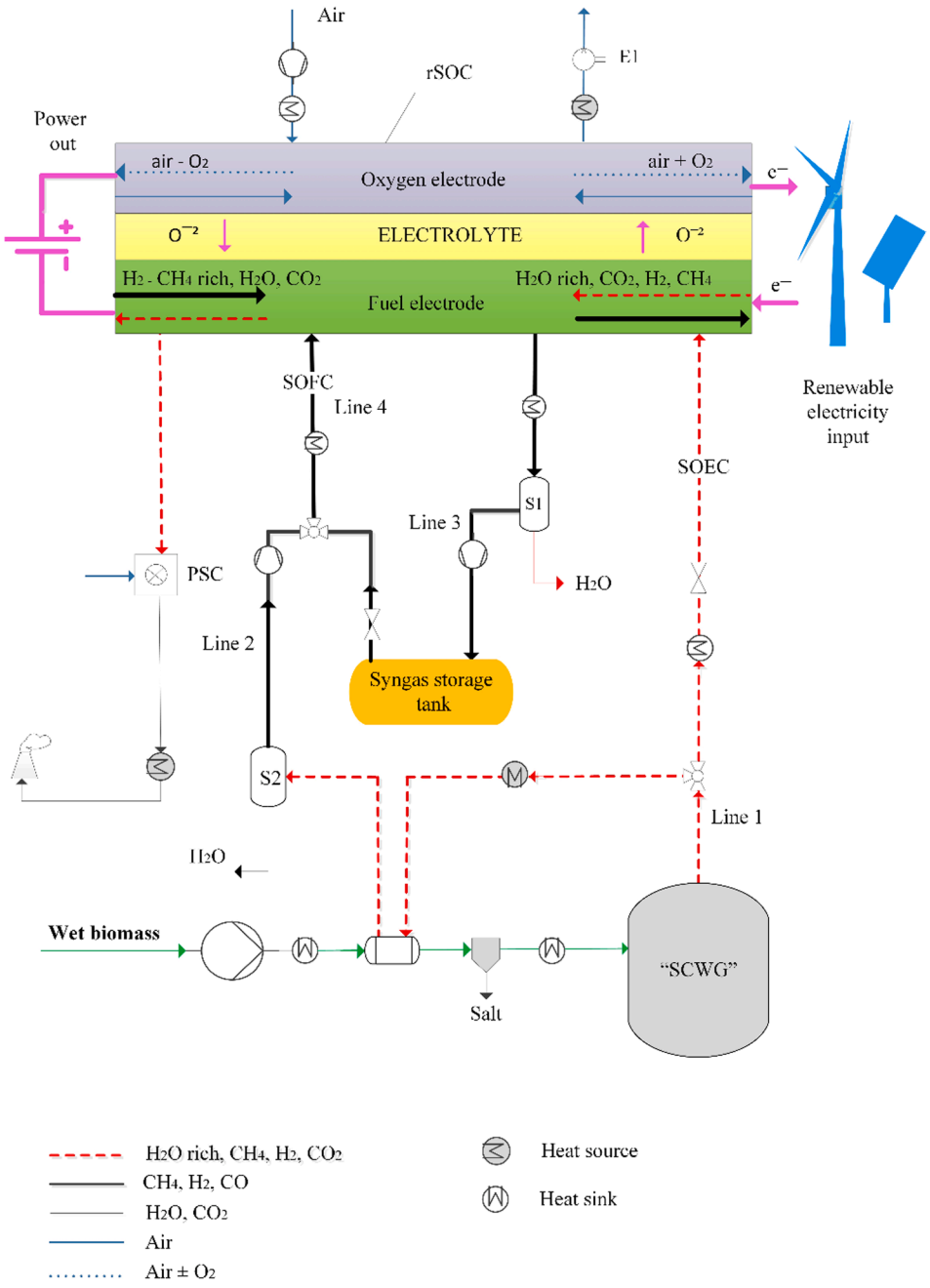

Fig. 1. Feed system of the SCWG–rSOC process.

destruction. The integration enables intermittent syngas or power production from wet biomass SCWG. Syngas generation from wet syngas generated in SCWG using an rSOC in EL mode, and power generation from mixed syngas using an rSOC in FC mode. In addition, by aligning with the objectives towards the sustainable development of society, this novel system can be a potential solution that addresses a threefold need: sustainable sanitation, power generation from wet biomass waste, and energy storage.

To evaluate the performance of the SCWG–rSOC system, process simulations were conducted. The efficiency of the combined system in each mode was calculated. The effects of several parameters such as biomass moisture content, rSOC stack temperature and pressure, and current density on the system efficiency were studied. Finally, an exergy analysis was carried out to identify the sources of greatest exergy destruction.

2. System concept

2.1. Integration of SCWG with rSOC

Fig. 1 shows a feed diagram of the proposed system, in which wet biomass is used to feed an endothermic SCWG. The gasifier generates a steam-rich gaseous mixture (Line 1, in Fig. 1) under supercritical water conditions. The rSOC stack operating in the electrolyser mode is directly fed with the pressure-regulated gaseous mixture coming from (Line 1, in Fig. 1) of the SCWG. Fig. 2A shows the process heat integration of the SCWG-rSOC EL mode. The high-temperature and high-pressure steam and CO_2 in the gaseous mixture are recovered and electrochemically reduced into H_2 and CO in the fuel electrode of the SOEC using electricity from the grid, which can be produced by solar and/or wind power systems. The heat required for the SOEC can be partly obtained from the heat generated by *in situ* methanation and partly from the heat generated

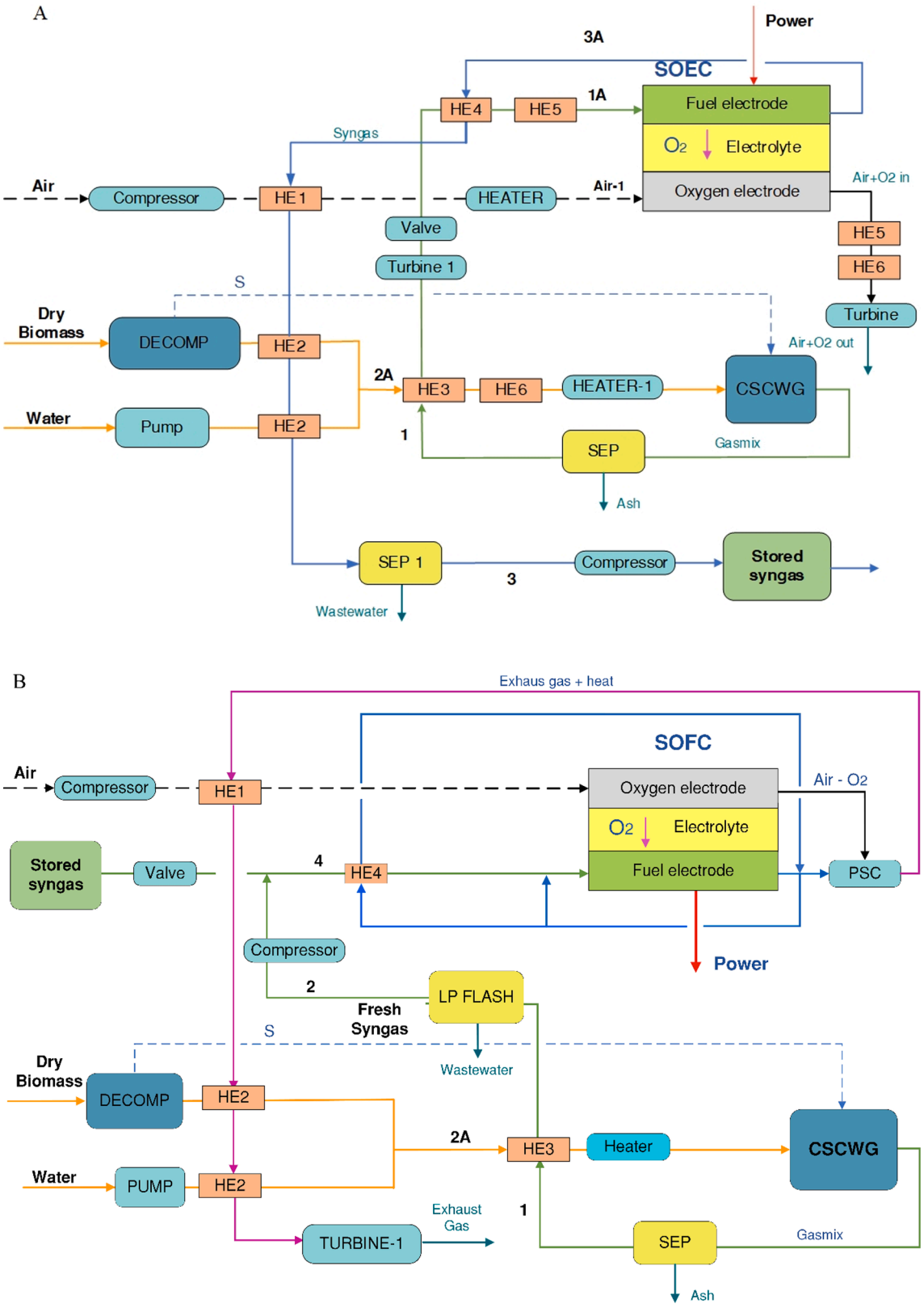

Fig. 2. Aspen Plus SCWG–rSOC feed system simulation. A) SCWG-rSOC-EL Mode, B) SCWG-rSOC-FC Mode.

from the rSOC losses (cell overpotential). Additional heat can be supplied by an external thermal source and process heat. An air stream feeds the oxygen electrode and is used as a sweep gas to remove the oxygen generated during electrolysis. The air stream is also used as a sink or source of heat for exothermic or endothermic SOEC operation. The expander E1 recovers any energy from the hot airflow. The SCWG is highly endothermic; heat exchangers are employed to facilitate the heat flow from the high temperature stream to the low temperature feedstock.

After SOEC operation, the unconverted H_2O is condensed in

Table 2
Main biomass properties.

Parameters	
Ultimate Analysis biomass (wt.%-dry basis)	[44]
H	6.3
C	49.1
N	5.9
S	2.0
O (by difference)	36.7
Proximate analysis (wt.% dry basis)	[44]
Volatile fraction (%, db)	46.46
Ash (%, db)	49.03
Moisture content (%, fresh weight)	90–95
Energy content LHV (dry), (MJ/kg)	16.84

separator S1 upon cooling to remove it from the fuel gas produced in the electrolyser. It is then pressurizer and stored in a tank for future use.

In the SOFC operation mode, two fuel sources are fed to the fuel electrode of the rSOC: the syngas from the SOEC, which is stored in the storage tank (Line 3 in Fig. 1), and the fresh syngas from the SCWG (Line 2 in Fig. 1), which is upgraded in a gas/liquid separator (S2) that removes the water from the gaseous mixture. The gaseous mixture is pressure-regulated before being fed to the SOFC stack, where the process heat preheats the fuel and air streams. Then, the gaseous mixture is electrochemically oxidised on the fuel electrode of the SOFC, producing electricity, heat, and exhaust compounds. The airflow provides oxygen for the electrochemical reactions and regulates the stack temperature, removing excess heat. Combustion takes place in the post-combustor (PSC) between the high-temperature airflow from the oxygen electrode and the exhaust species from the SOFC fuel electrode. Fig. 2B shows the process heat integration of the SCWG-rSOC FC mode.

Main assumptions of this study are:

- All processes are in steady-state equilibrium; the system is well insulated (i.e. no energy or exergy is lost to the environment from the process units).
- Low solubility of the inorganic compounds (ash) in supercritical water at thermodynamic equilibrium·NH_3 and SO_2 is transported by water in the gas–liquid separation units [39].
- Co-electrolysis of H_2O and CO_2 takes place at the fuel electrode of the rSOC in EL mode [40,41].
- The ASR estimation uses a gaseous mixture of H_2O and H_2 [42].
- External heat supplied to the system is electric heat.

3. Thermodynamics of the SCWG–rSOC system

3.1. Chemical analysis

Non-traditional biomass feedstocks such as wet animal manures, human waste, sewage sludges, food industry waste, aquaculture residues and algae are potential feedstock for SCWG. These feedstocks are large renewable residual streams, continuously generated. These feedstocks must be treated to guarantee the protection of the environment. However, the high degree of heterogeneity in the form, composition and water content of biomass is a disadvantage for almost all applications [43]. Real biomass is quite challenging due to the complex nature containing cellulose, hemicellulose and lignin. For the SCWG, equations (1,2) describe the complete conversion of biomass into a mixture of H_2, CH_4 and CO_2, where the organic matter of biomass is assumed as $C_6H_{12}O_6$ as a representative model biomass compound used to understand the gasification process. Table 2 shows a sample composition of the biomass. We assume low solubility of the inorganic compounds (ash) in supercritical water at thermodynamic equilibrium [39]. It is separated in the salt separator unit, Fig. 1.

The sulphur content is converted to H_2S, while nitrogen content is converted to NH_3 [45]. The addition of a ZnO bed in the reactor allows the removal of H_2S [17,18] in the SEP unit described in Fig. 2A and 2B·NH_3 is assumed to be transported by water in the SEP 1 and LPFLASH water separation units in Fig. 2A and 2B, respectively. The temperature, pressure, residence time, and amount of water in the biomass all influence the product gas composition. Furthermore, hydrogen production is favoured at high temperatures, whereas methane generation is facilitated by high pressures [46]. Note that the reaction in Equation (2) is exothermic and thus contributes to reducing the heat required for the gasification process.

$C_6H_{12}O_6 + 6H_2O \rightarrow 6CO_2 + 12H_2\ \Delta H = 360\ \mathrm{kJ{\cdot}mol^{-1}}$ (1).

$C_6H_{12}O_6 \rightarrow 3CH_4 + 3CO_2\ \Delta H = -132\ \mathrm{kJ{\cdot}mol^{-1}}$ (2).

Details of the thermodynamic analysis of the FC operation mode can be found in [34]; the analysis of electrolysis and thermochemical reactions is detailed in Equations (3)–(9). The excess electrical energy—available from renewable sources—and a residual heat supply (external or internal) serve as energy inputs for high temperature electrolysis. Equations (3) and (4) represent the reduction of H_2O and CO_2; thus, electrical energy is stored in the chemical form. The generated CO and H_2 react to form methane following Equation (8) (methanation reaction) at low temperature and high pressure (600 °C, 20 bar). Methanation has a considerable impact on cell thermal management because of the relatively high amounts of heat released (ΔH) due to its exothermic nature [47], which contribute to satisfying the heat requirements of the SOEC. Operating conditions also allow the reverse water–gas shift reaction (the reverse of Equation (7)) to be predominant, which results in the reduction of CO_2 by H_2 [48].

Full cell reactions in the rSOC:

$$H_2O(\mathrm{gas}) \leftrightarrow H_2 + 1/2O_2 \qquad \Delta H = 242\ \mathrm{kJ\hat{A}{\cdot}mol^{-1}} \tag{3}$$

$$CO_2 \leftrightarrow CO + 1/2O_2 \quad \Delta H = 283\ \mathrm{kJ\hat{A}{\cdot}mol^{-1}} \tag{4}$$

Reactions at the fuel electrode:

$$H_2O + 2e^- \leftrightarrow H_2 + O^{2-} \tag{5}$$

$$CO + O^{2-} \leftrightarrow CO_2 + 2e^- \tag{6}$$

$$H_2O + CO \leftrightarrow H_2 + CO_2 \qquad \Delta H = -41\ \mathrm{kJ\hat{A}{\cdot}mol^{-1}} \tag{7}$$

$$3H2 + CO \leftrightarrow CH4 + H2O(\mathrm{gas}) \qquad \Delta H = -206\ \mathrm{kJ\hat{A}{\cdot}mol^{-1}} \tag{8}$$

Reactions at the oxidant electrode:

$O^{2-} \leftrightarrow 1/2O_2 + 2e^-$ (9).

4. Energy analysis of the rSOC system

The overall energy required to spur a chemical reaction [49] in the rSOC is given by:

$$\Delta H_{\mathrm{SOEC}} = \Delta G + T\Delta S \tag{10}$$

where ΔH is the change in enthalpy; ΔG is the change in Gibbs free energy, which, at a constant pressure and temperature, determines the maximum value of the useful electrical work of the system required to initiate the reaction; and $T\Delta S$ is the product of the temperature and change in entropy, which determines the reversible transfer of heat.

The reversible cell voltage of the rSOC is related to ΔG through the Nernst equation as a function of the species partial pressure of the system. This equation represents a case in which an electrochemical reaction facilitates the charge transfer between phases [50]. This transfer of charged species (electrons or ions) across the interface in an rSOC depends on the amount and nature of the electrode/electrolyte/gas triple-phase boundaries (TPB). Assuming that co-electrolysis of H_2O and CO_2 takes place at the fuel electrode of the rSOC in EL mode [41], the reversible cell voltage, E_r, is the average of the Nernst equation applied to the chemical reactions in Equations (3) and (4) as follows [40]:

$$E_{r,H_2O} = E_{0,H_2O} + \frac{RT}{nF}\frac{p_{H_2}p_{O_2}^{1/2}}{P_{H_2O}} \quad (11)$$

$$E_{r,CO_2} = E_{0,CO_2} + \frac{RT}{nF}\frac{p_{CO}p_{O_2}^{1/2}}{p_{co_2}} \quad (12)$$

$$E_r = \frac{1}{x_{H_2O} + x_{CO_2}}\left(x_{H_2O}E_{r,H_2} + x_{CO_2}E_{r,CO}\right) \quad (13)$$

where the quantity nF expresses the amount of charge transferred for every mole of reactant species.

The reversible voltage calculated by the Nernst equation is equivalent to the open-circuit voltage (OCV), which can be measured as the difference between the electrode potentials of the anode and cathode when no current is flowing.

The rSOC reversible voltage varies with the electrical current flowing through the system, and its nature depends on the direction of the current [50].

Resistance to the flow of charge in a cell leads to Ohmic losses. The charge transfer reactions cause activation losses, whereas the transport limitations of gases through the porous electrodes to the TPB cause concentration/diffusion losses. These resistances affect the final voltage of the rSOC. Thus, the operating voltage is higher than the OCV for the case of an SOEC as follows:

$$V_{SOEC} = E_r + \eta_a(j) + \eta_{ohm}(j) + \eta_{conc}(j) \quad (14)$$

The total overvoltage η is equal to the area-specific resistance (ASR) times the current density of the cell, resulting in the following expression for SOEC operating voltage [51]:

$$V_{SOEC} = E_r + ASR^*j \quad (15)$$

For the ASR estimation, it is assumed that the rSOC stack is fed with a gaseous mixture of H_2O and H_2. The SOEC stack ASR is described using the models developed by [52] and [42]. Table A1 provides the simulation parameters to fit the I-V curve of a two-electrode supported solid oxide cells with structure of "Ni-Sm doped CeO_2 infiltrated porous $La_{0.9}Sr_{0.1}Ga_{0.8}Mg_{0.2}O_3$ (LSGM) dense LSGM/$SmBa_{0.5}Sr_{0.5}CO_2O_5$ infiltrated porous LSGM" tested in the work of Wang S. et al. at 600 °C [53]. Appendix A gives supplementary information about ASR estimation.

5. Current density

When operating in EL mode, the amount of current through the external circuit depends on whether reduction of CO_2 at the fuel electrode occurs through steam electrolysis followed by reverse water–gas shift reaction or via direct co-electrolysis. It also depends on structural and operational parameters, which determine if direct CO_2 electrolysis will have a significant or negligible influence on the process [42]. According to [54], a surface ratio β, derived based on the applied experimental method, splits the active surface area for the H_2O and CO_2 electrochemical reductions. In this study, the approach of [40] was considered which is as follows:

$$I_{SOEC/H_2O} = 2F\dot{n}\beta \bullet U_f \quad (16)$$

$$I_{SOEC/CO_2} = 2F\dot{n}(1-\beta) \bullet U_f \quad (17)$$

$$\beta = \frac{y_{H_2O}^{TPB}}{y_{H_2O}^{TPB} + y_{CO_2}^{TPB}} \quad (18)$$

The current density is estimated by: has.

$$j_{SOEC} = \frac{I_{SOEC}}{A_{SOEC}} \quad (19)$$

A single SOEC stack consisted of parallel connected cells. Each cell of the SOEC has an active area equal to 0.1 m^2. For each biomass moisture content, the required number of cells is obtained with the objective of operating the cell with the highest system efficiency.

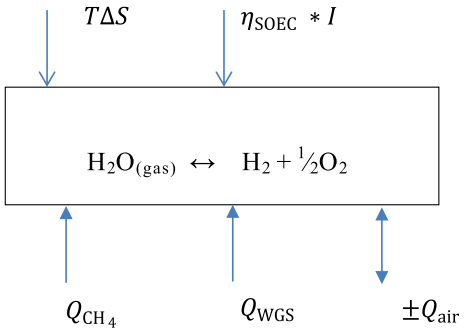

Fig. 3. rSOC electrolysis mode heat balance.

The power supplied to the electrolysis operation can be calculated by:

$$P_{SOEC} = V_{SOEC} \bullet I_{SOEC} \quad (20)$$

6. Thermoneutral voltage

The theoretical thermoneutral voltage in electrolysis mode is obtained as [48]:

$$V_{TN} = \frac{\Delta H_{SOEC}}{nF} \quad (21)$$

In SOEC mode, V_{TN} is the cell voltage provided to the SOEC system. The heat generated in the cell meets the heat balance of all cell reactions, both chemical and electrochemical [48], thereby resulting in both adiabatic and isothermal operations [55]. At operating voltages less than or greater than V_{TN}, the system operates in the endothermic mode or the exothermic mode, respectively. The molar change of the enthalpy ΔH of the reactions promoting charge-transfer (Equations (3) and (4)) depends on the external supply of power, ΔG, and heat, $T\Delta S$, as expressed in Equation (10). The energy balance diagram of the SOEC shown in Fig. 3 depicts all the energy (heat and power) sources and sinks influencing the thermal energy required by the reactions defined in Equations (3) and (4).

In Fig. 3, Q_{CH_4} and Q_{WGS} are the reaction enthalpies of the spontaneous reactions for methanation and water–gas shift, respectively, at the fuel electrode. The heat liberated by the cell losses is equal to the overpotential, η_{SOEC}, times the current, I. The air fed to the air electrode acts as a temperature regulator, adding or removing heat, Q_{air}, from the SOEC. Thus, based on the energy balance equation, Q_{air} can be computed by:

$$Q_{air} = T\Delta S - (Q_{CH_4} + Q_{WGS} + \eta_{SOEC}I) \quad (22)$$

Combining Equation (22) with Equations (10) and (14) results in.

$$Q_{air} = \Delta H_{SOEC} - V_{SOEC} \bullet I - (Q_{CH_4} + Q_{WGS}) \quad (23)$$

The Aspen Plus™ reactor blocks provide the values for Q_{CH_4}, Q_{WGS}, and ΔH_{SOEC}. When $Q_{air} = 0$, the SOEC is in thermoneutral mode, and the operating voltage is equal to the thermoneutral voltage. In this case, the oxygen electrode supplies a small amount of air to release the product O_2, since there is no heat to provide to or remove from the SOEC. When $Q_{air} > 0$, the net operation in the SOEC is endothermic, and air at a higher temperature than the SOEC operating temperature provides the heat required by the cell. When $Q_{air} < 0$, the net SOEC operation is exothermic and sweep air at a lower temperature than the SOEC operating temperature drains the excess heat.

7. Exergy analysis of the SCWG-rSOC system

Eq. (24) describes the exergy balance of the SCWG–SOEC system at

steady state [56]. The exergy enters the system in the form of biomass and electricity. The system is well insulated; there is no exergy transfer accompanying heat transfer.

$$0 = \dot{W}_{cv} + \sum_{i} \dot{m}_i e_{fi} - \sum_{e} \dot{m}_e e_{fe} - \dot{E}_d \quad (24)$$

The total specific flow exergy is the sum of the thermomechanical and chemical exergies:

$$e = e_f + \overline{e}^{ch} \quad (25)$$

The thermochemical exergy is given by:

$$e_f = h - h_0 - T_0(s - s_0) \quad (26)$$

The chemical exergy for an ideal gaseous mixture at the reference environment (T_0, p_0) is given by:

$$\overline{e}^{ch} = \sum_{i} (y_i \overline{e}_i^{ch} + y_i \overline{R} T_0 \ln y_i) \quad (27)$$

8. Efficiency definitions

The SCWG–rSOC system's efficiency:

$$P_{BOP,system} = ÆP_{heat} + ÆP_{power} \quad (28)$$

P_{heat} is the external heat supplied to the system (heaters), assuming electric heat, and P_{power} is the power of the auxiliary components (pumps, gas compressors). Aspen Plus™ blocks provide values for each P_{heat} and P_{power} component of the system. In the equations below, the subscript (i) refers to the components relevant to the subsystem whose efficiency is being calculated.

SCWG efficiency:

$$\eta_{SCWG} = \frac{\dot{m}_{fuel} LHV_{syngas,SCWG}}{\dot{m}_{biomass} LHV_{biomass} + P_{BOP,(i)}} \quad (29)$$

$$\eta_{ex-SCWG} = \frac{Ex^{ch}_{syngas} + Ex^{f}_{gasmixture}}{\dot{m}_{biomass} Ex^{ch}_{biomass} + P_{BOP,(i)}} \quad (30)$$

rSOC efficiency:

$$\eta_{SOEC} = \frac{\dot{m}_{fuel} HHV_{syngas,SOEC} - \dot{m}_{fuel} HHV_{syngas,SCWG}}{P_{SOEC} + P_{BOP,(i)}} \quad (31)$$

$$\eta_{SOFC} = \frac{P_{SOFC} - P_{BOP,(i)}}{\sum \dot{m}_{fuel} HHV_{syngas,(i)}} \quad (32)$$

The system energy efficiency:

$$\eta_{SCWG-SOEC} = \frac{\dot{m}_{fuel} HHV_{syngas,SOEC} - \dot{m}_{biomass} HHV_{biomass}}{P_{SOEC} + P_{BOP,system}} \quad (33)$$

$$\eta_{SCWG-SOFC} = \frac{P_{SOFC} - P_{BOP,system}}{\dot{m}_{fuel} HHV_{syngas,SOEC} + \dot{m}_{biomass} HHV_{biomass}} \quad (34)$$

Exergy efficiency of the system:

$$\eta_{ex-SCWG-SOEC} = \frac{Ex^{ch}_{syngas} - Ex^{ch}_{biomass}}{P_{SOEC} + P_{BOP,SCWG-SOEC}} \quad (35)$$

$$\eta_{ex-SCWG-SOFC} = \frac{P_{SOFC} - P_{BOP,SCWG-SOFC}}{Ex^{ch}_{syngas,SOEC} + Ex^{ch}_{biomass}} \quad (36)$$

9. Simulation of the CSCWC rSOC model in Aspen Plus™

Fig. 2A and 2B depict the feed system model of the SCWG–rSOC operation as simulated on Aspen Plus™. The rSOC model was built based on the work in [58,59,60]. This model considers the following assumptions: all processes are in steady-state equilibrium; the system is well insulated, and no energy or exergy loss occurs in the process units.

Table 3
SCWG operating conditions.

Parameter	
SCWG	
Temperature (°C)	500
Pressure (bar)	250
Biomass mass flow rate (dry) (g/s)	0.56
Biomass water flow rate (80, 90, 95 wt%) (g/s)	2.24, 5.04, 10.64
HP-LP flash pressure (bar)	10–1 [45]
HP-LP flash temperature (°C)	100–25 [45]
Pump isentropic efficiency (%)	85 [57]
Biomass moisture content (wt.%)	95
Energy biomass input (on HHV) (kW)	8.92
Energy biomass input (on LHV) (kW)	8.25
Exergy biomass input (kW)	10.56

Table 4
rSOC operating conditions.

Parameters	
rSOC	
Temperature (°C)	680–850
Pressure (bar)	1–20
Fuel utilization	0.95–0.65
Number of cells	260–370
Area of a cell (m2)	0.01
Current density SOFC (A cm^{-2})	<2
Current density SOEC (A cm^{-2})	>2
Storage fuel tank temperature (°C)	25
Storage fuel tank pressure (bar)	400 [61]
DC/AC inverter efficiency (%)	95 [62]
Fuel compressor isentropic efficiency (%)	85 [57]
Air compressor isentropic efficiency (%)	85 [57]
Heat exchanger minimum approach temperature (°C)Process units	10
pressure drop (bar) *	0.02

* Each process unit of SCWG–rSOC system.

The Aspen model consists of three sections: SCWG, SOFC, and SOEC. In the SCWG, the gasifier model uses the procedure available in the Aspen Plus process simulation using solids. Table 3 lists the operating parameters of the SCWG. The RGibbs block used to represent the SCWG predicts the final gas product concentration from the gasifier based on the minimisation of the total Gibbs free energy. Table 2 lists the elementary composition of the dry biomass described by the Dry biomass stream, Fig. 2A and 2B. The biomass decomposes into its constituent elements in the RYield block, DECOMP, at ambient temperature and a pressure of 250 bar. The heat of reaction, which is a product of the decomposition of the biomass, is considered in biomass gasification. Heat stream S then carries the reaction heat from the RYield block to the RGibbs block in the SCWG. The WATER stream is used to simulate the water content of the biomass. The pressure of the WATER stream is increased to 250 bar at PUMP and mixed with decomposed biomass stream 2A. The heat exchangers HE2, HE3 and HE6 and HEATER-1 preheat solution stream 2A, and the preheated species enter the reactor SCWG. The GASMIX fuel stream is then directed to either the SOFC or SOEC block, depending on the desired operation mode defined by the availability of electricity.

In the SOFC, as shown in Fig. 2B, the SOEC stored syngas and the fresh syngas from the SCWG (stream 2) are mixed to form stream 4, and fed into the system. The turbine TURBINE-1 recovers part of the energy from the exhaust. For a complete discussion of the SCWG–SOFC simulation, the reader is referred to [34].

The SCWG-rSOC-EL model is shown in Fig. 2A and Table 4 provides the operating parameters of the rSOC. The SCWG-rSOC-EL model (see Figure S1 supplementary material) employs three blocks to describe the fuel electrode: WGSR, CATHODE, and METH. The RGibbs blocks WGSR and METH account for the heterogeneous reactions on the catalytic

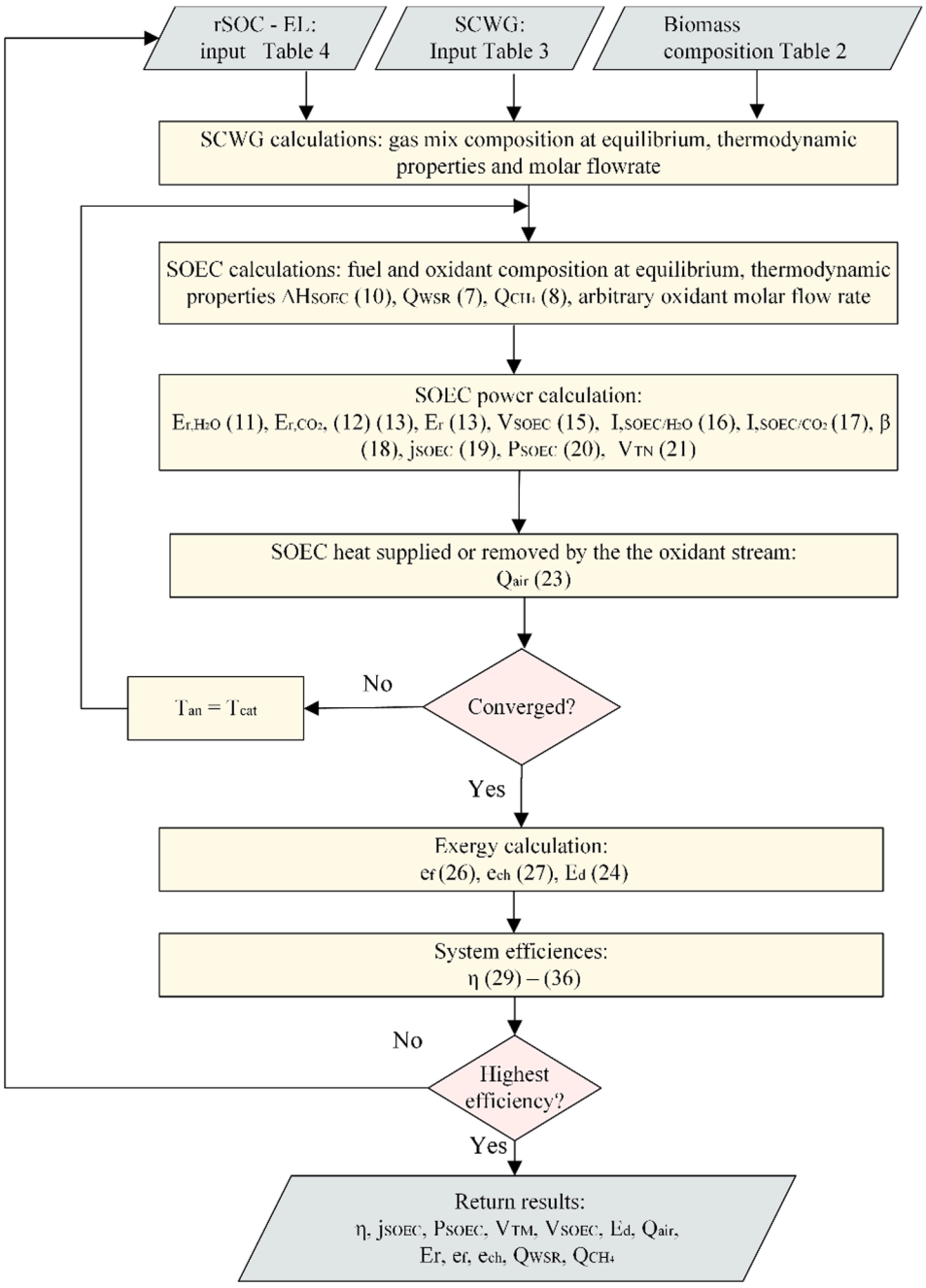

Fig. 4. Calculation workflow for estimating the highest efficiency of the SCWG-rSOC-EL (numbers in parentheses refer to equations in this paper).

material of the fuel electrode: the forward and reverse water–gas shift reaction (WGSR) and methanation reaction (METH). The stoichiometric block CATHODE defines the electrochemical reduction of H_2O and CO_2 into O_2, H_2, and CO. The separator block ANODE1 and heater Q6 simulate the air electrode. The block ANODE1 separates the oxygen and syngas from CATHODE. The heat in the fuel electrode is added to or removed from the SOEC using block heater Q6. An Aspen Fortran calculator computes total heat entering or leaving block Q6 according to the energy balance shown in Fig. 3 and defined in Equation (23). The airflow rate of the stream AIR and temperature of stream 17 by means of electric heater Q7 changes to keep the temperature of the outlet air stream 18 equal to the SOEC operating temperature.

The enthalpy of the electrochemical reaction is estimated using the net DUTY of CATHODE. The enthalpy of the heterogeneous reactions, WGSR, and METH are determined by the DUTY of block WGSR and METH, respectively. The calculation sequence for estimating the efficiency of the is shown in Fig. 4.

10. Results and discussion

10.1. rSOC results comparison

The ASR of the rSOC is compared with the experimental I-V curve presented by Wang et al. [53] as shown in Fig. 5A and Fig. 5B. Table 1A provides the fitted cell parameters to obtain the experimental results. The model accurately simulated the rSOC experimental results of Wang, at 600 °C, at atmospheric pressure 50 % H_2O and 70 % H_2O. The higher the gas concentration, the higher the cell exchange current density [63]. This is reflected in the variation of the slope curve.

The predicted value of the ASR, rSOC operating at 20 bar, 680 °C and

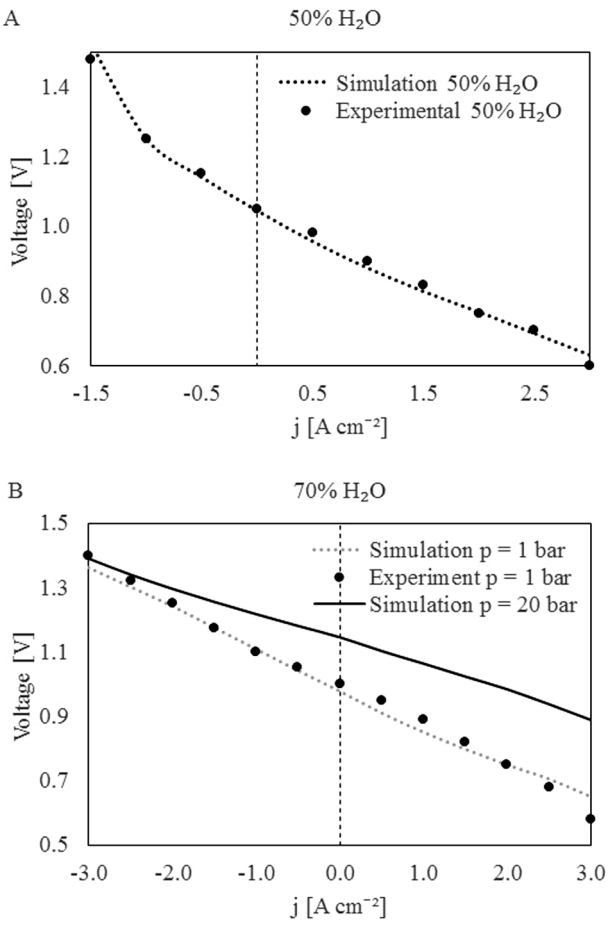

Fig. 5. A - B Experiments by Wang et al. [53] and present simulation results.

70 % H_2O is shown in Fig. 5B. Concentration losses in the SOEC are reduced at higher operating pressure and higher H_2O concentration, while the increased temperature reduces Ohmic losses. Therefore, increasing pressure, gas concentration and temperature are favourable for the rSOC performance, obtaining stable ASR, which is shown in Fig. 5B. This trend coincides with the results presented in the work of Hauck et al. [42]. The ASR value of rSOC, at temperature > 800 °C and ambient pressure, used in this work is equal to the value presented by Banner et al. [64] for LNO-LDC50 and LSM-YSZ oxygen electrodes. As a result, the following analysis uses an ASR in the range of 0.11 to 0.16 Ω cm^{-2}.

At 95 wt% biomass moisture, the pH_2O/pCO_2 ratio of the gas mixture SCWG (see Table 5) is around 53. According to recent findings of Ioannidou et al. [65], the H_2O/CO_2 co-electrolysis process in $pH_2O/pCO_2 = 1$ is 100 % selective towards H_2O electrolysis. A similar behaviour is expected at pressurized operation [66]. Therefore, the influence of CO_2 electrochemical reduction is negligible for 95 wt% biomass moisture. The surface ratio β is almost one calculated with Eq. 18.

The exergy efficiency of the SOEC at 95 wt% biomass moisture, 1 bar and 850 °C, (see Table 6) is 78 %. This value is in agreement with the findings of [67]. At 20 bar and 680 °C, feedstock with a moisture content of 80, 90 and 95 wt% the thermoneutral voltage found in this work is in the range of 1.24–1.25 V and the reversible voltage is around 1.1 V. These values are in the same range of the findings of [48] at 20 bar and H/C ratio higher than 40.

11. SCWG-rSOC operation

The performance analysis of the proposed SCWG-rSOC system based on energy, exergy, and mass balances for power or syngas generation (i.e., FC mode and EL mode, respectively) are summarized here. The performance is studied by making use of an exergy flow diagram, which indicates the exergy losses occurring in the various processes; the diagram also indicates additional external heat requirements, process heat recovery and the power consumed by the auxiliary units. Subsequently, the changes in the energy efficiency of the SCWG-rSOC are analysed as a function of i) biomass moisture, ii) rSOC pressure, iii) rSOC temperature, iv) syngas flow rates, v) current density. Table 5 reports the key data describing the system performance. Fig. 6 shows a schematic of energy/exergy flows of the SCWG-rSOC in FC and EL mode. Fig. 7 A-C shows the flowsheet of the system and Table 5 present the main gas compositions. The thermochemical and chemical exergy flows are shown in Fig. 7, at $j = 3.4$ A cm^{-2}, $T = 680$ °C, $P = 20$ bar, biomass moisture content = 95 wt %.

12. SCWG-rSOC operating in EL mode

Fig. 8A shows an exergy flow diagram of the results of the performance analysis of the syngas generation. The system is fuelled by SCWG product gas mixture (Line 1 in Fig. 1) and electricity, and the system generates biofuel (Line 3 in Fig. 1). Table 5 summarizes the results of analysis of flow rates, gas composition, pressure, temperature of the gases labelled in Fig. 1, Line 1. In Fig. 8A and Table 5, the SCWG–rSOC EL operation is at $j = 3.4$ A cm^{-2}, $T = 680$ °C, $P = 20$ bar, and biomass moisture content = 95 wt%.

Table 5
Performance results of SCWG-rSOC.

Chemical composition										
		Gas mix. SCWG		Fresh SCWG syngas		SOEC syngas	Mixed gas			
Stream in Fig. 2A		Line 1	Line 1A	Line 2	Line 3A	Line 3	Line 4	Air-1	Air + O2 in	Air + O2 out
H_2	%mol	1.6	1.6	29.0	73.0	95.3	90.7	–	–	–
CH_4	%mol	1.4	1.4	26.2	3.3	4.4	5.8	–	–	–
H_2O	%mol	95.1	95.1	9.9	23.5	0.1	0.8	–	–	–
CO_2	%mol	1.8	1.8	33.4	trace	trace	2.3	–	–	–
CO	%mol	trace	trace	–	trace	trace	–	–	–	–
NH_3	%mol	trace	trace	–	trace	trace	–	–	–	–
N_2	%mol	trace	trace	1.28	trace	trace	0.16	71.0	67.1	67.1
O_2	%mol	–	–		–	–	–	21.0	32.9	32.9
Total flow	mol s^{-1}	0.611	0.611	0.033	0.589	0.451	0.48	1.309	1.541	1.541
	g s^{-1}	11.1	11.1	0.726	3.7	1.2	1.94	37.8	45.2	45.2
LHV (ref. 15 °C)	kJ mol^{-1}	15.4	15.4	280.9	203.5	265.7	266.7	–	–	–
Chemical exergy	kJ mol^{-1}	15.5	15.5	300.4	198.6	261.1	262.4	–	–	–
Temperature	°C	500	680	97	680	25	680	569	680	−12
Pressure	bar	250	20	1.013	20	20	20	20	20	1.013
Specific Enthalpy	kJ mol^{-1}	−226.7	−214.2		−38.6	−3.7		16.6	20.3	−1.1

Table 6
Key data – SCWG-rSOC performance.

Parameter	Unit	SCWG-rSOC-FC	SCWG-rSOC-EL	SCWG-SOFC	SCWG-rSOC-FC	SCWG-rSOC-EL	SCWG-SOFC
Reactant		Mix syngas	Gas mixture	Fresh syngas	Mix syngas	Gas mixture	Fresh syngas
SOC operating pressure	bar	1			20		
SOC operating temperature	°C	850			680		
rSOC ASR	Ω.cm^{-2}	0.11			0.16		
SCWG Exergy efficiency	%	76.4	69	68.9	32.4	78.1	61.4
Individual mode simulations							
Current density	A cm^{-2}	1.5	3.4	0.13	1.5	3.4	0.14
Stack active area	cm^{-2}	60,000	26,250	60,000	60,000	26,250	60,000
Turbine net power production	kW				56	9.6	
SOFC net power production (AC)	kW	80.42		6.8	64		7.76
SOFC net power production (DC)	kW	84.65		7.2	68		8.17
SOEC fuel production (on HHV)	kW		147			145	
SOEC fuel production (on LHV)	kW		124			124	
System efficiency (on HHV)	%	56.4	87	57.8	42	89	21.0
System efficiency (on LHV)	%	65.9	73	62.6	46	77	22.7
System exergy efficiency	%	61.6	70	52.3	49	73	48.8
Exergy efficiency rSOC-FC/EL	%	59.4	77.9	68.5	72.6	74.5	70
System with same area in both modes							
Current density	A cm^{-2}	2.7			2.7		
Stack active area	cm^{-2}	33,750			33,750		
Energy efficiency of the system	%	44.9	88.56		31.1	88.4	

Table A1
Simulation parameter of the SOC.

Parameter		Unit	Fit. Value	Ref.
Anode - cathode				
Thickness anode	dan	μm	2.10E-04	[53]
Thickness cathode	dcat	μm	2.10E-04	[53]
Particle diameter	d_p	[nm]	200	[53]
Porosity	ε		0.3	[52]
Tortuosity	τ		5	[52]
Empirical constant	$i^*_{H_2}$	A/cm2	2.8	[52]
Pre-exponential of desorption	A_{des}	s cm2/mol	5.59E + 19	[52]
Surface site density	Γ	mol/cm2	2.60E-06	[52]
Sticking probability	γ_0		0.01	[52]
Activation energy of desorption	E_{des}	kJ/mol	88.12	[52]
Empirical constant	i^*_{O2}	A/cm2	0.4	
Pre- exponential factor	A_{O_2}	atm	4.90E + 08	[52]
Activation energy	E_{O_2}	kJ/mol	200	[52]
Electrolyte				
Thickness	del	μm	1.60E-05	[53]
Pre- factor of O^{2-}	so,el	W-1 cm-1	333.3	[52]
Activation energy	E_{el}	J/mol	85.63	[52]

The system efficiency depends on the external power and heat supplied to the system, and the efficient utilisation of the process heat in the SCWG fuel, air, and fuel preheating. The generated process heat almost satisfies the heat required by the SCWG, fuel and air preheaters. The energy supplied to the electrolyser is used to electrochemically reduce steam and CO_2 from the gas mixture, generating H_2 and CO (syngas). The use of rSOC in EL mode results in an amount of syngas (Line 3, Fig. 1) that is around thirteen times the fresh syngas generated exclusively in the SCWG gasifier (Line 2, Fig. 1). Some energy is recovered as electricity using the turbine, although with high exergy destruction. The fuel generated by the SCWG-rSOC system in EL mode contains approximately 69 % of the total exergy input to the entire system. The exhaust gas emitted to the environment is at ambient temperature, thus its exergy loss (that eventually becomes exergy destruction in the atmosphere) is negligible. In contrast, the exergy destruction of the electrolyser and turbine (9.6 and 6.4 kW respectively) have significant influence in reducing the system performance. The rSOC stack in EL mode must operate at a current density higher than 2 A·cm^{-2}. This current density was derived considering that the system must operate near the thermoneutral voltage to attain the highest possible efficiency. The system achieves an energy efficiency of 91 % which can be compared with and efficiency of biomass and electricity by gasification with pressurized SOEC of 84 % [9].

13. SCWG-rSOC FC operation

Fig. 8B shows an exergy flow diagram of the results of the performance analysis of the SCWG-rSOC operating in FC mode for power generation. In Fig. 8B and Table 5, the SCWG–rSOC FC operation is at j = 3.4 A cm^{-2}, T = 680 °C, P = 20 bar, biomass moisture content = 95 wt %. The fuel used can either be: Part i) only syngas produced by SCWG (while system is running in FC mode), hereafter called "fresh syngas" Part ii) fresh syngas + stored syngas which was produced in rSOC in EC mode. This mixture is hereafter called "mixed syngas".

Table 5 summarizes the results of flow rates, gas composition, pressure, temperature of the gases labelled in Fig. 1 as Line 2 and Line 3. Fig. 8C and Table 5 shows the results of the analysis of power generation by the rSOC in FC mode fuelled exclusively by fresh syngas (Lines 2 in Fig. 1).

It can be seen from Fig. 8B and Fig. 8C, that the twelve times higher power is produced when the rSOC uses mixed syngas, when compared with using only fresh syngas. This is owing to the higher flow rate of the mixed syngas, as well as its higher calorific value. The rSOC fuelled by the mixed syngas has higher exergy losses and exergy destruction than the rSOC fuelled by fresh syngas. This is because the system fuelled by the mixed syngas is not configured for optimal utilisation of the heat produced in the rSOC and PSC. Therefore, improving the heat integration can have a scope for significant reductions in the exergy losses and exergy destruction. The current density was derived considering the amount of produced heat to be distributed in the system to reach the minimum exergy loss and destruction in the exhaust and process units respectively.

14. Sensitivity analysis of SCWG-rSOC FC operation

14.1. Effect of pressure and temperature and moisture content on the energy efficiency of the SCWG-rSOC FC mode system

Fig. 9A shows the influence of the operating pressure and temperature of the rSOC on the energy efficiency of the SCWG–rSOC system in FC mode, at biomass moisture contents of 80 and 95 wt%, with current densities of 0.47 and 1.5 A·cm^{-2}, respectively. The feed to the rSOC consists of the "mixed syngas".

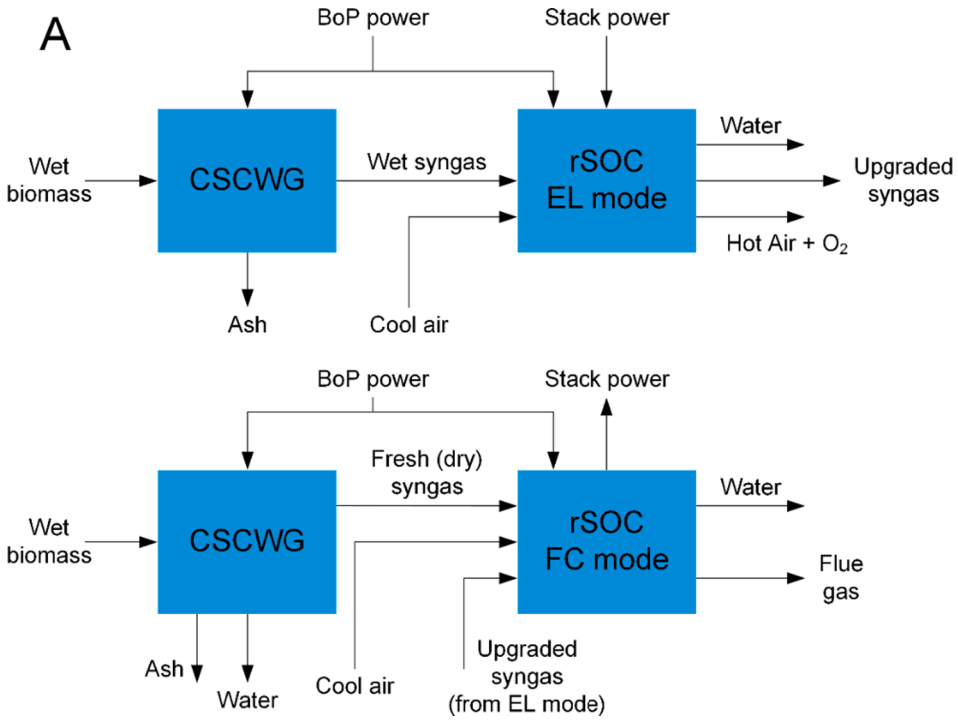

Fig. 6. Schematic for energy/exergy flows in each mode.

At a high biomass moisture content (95 wt%) the gasifier was endothermic because the high moisture content favours the production of H_2, which is an endothermic reaction. The energy consumed by the gasifier under this condition was approximately 2 kW. However, at a moisture content of 80 wt%, the gasifier was exothermic and generated 0.453 kW of heat since low moisture promotes the exothermic methanation reaction. Additionally, the energy required by the gasifier preheater to take the biomass to the reaction temperature was exceptionally high at 95 wt% moisture, due to high flow rates.

High operation pressures increased the rSOC power output due to the higher Nernst voltage. The external heat demand for the preheating of air and fuel decreased because of the increase in gas temperatures caused by the air and fuel compressors, respectively. However, the adverse effects of increased compressor power requirements overrode both these benefits, and the overall system efficiency decreased.

The reduction in efficiency with increasing stack pressure was more severe at 95 wt% moisture content than at 80 wt% because, at 95 wt%, the air compressor required more power to remove excess heat from the rSOC. This was the result of greater heat generation in the stack at 95 wt % due to the higher fuel consumption rate. Indeed, at 95 wt%, the syngas molar flow rate was almost five times that at 80 wt% (0.48 $kmol{\cdot}s^{-1}$ compared to 0.1 $kmol{\cdot}s^{-1}$) because as mentioned before, the mass flows are higher at higher biomass moisture levels. The higher fuel consumption also required a higher current density (0.47 $A{\cdot}cm^{-2}$ at 80 wt% and 1.5 $A{\cdot}cm^{-2}$ at 95 wt%) that increased the overpotentials, further contributing to greater heat generation in the rSOC at higher biomass moisture contents.

At 80 wt%, the reduction in efficiency with increased pressure was less severe at 850 °C than at 680 °C because a high temperature favours the endothermic reformation of methane in the rSOC, reducing the heat generation and thus requiring lower cooling airflow. At a lower airflow, the increase in compressor power with pressure was less severe, and so was the decrease in efficiency. At 680 °C, however, the opposite effect was observed: low temperature and high-pressure favour exothermic methanation, which increased the heat generation in the stack. Thus, the compressor power required to drive the cooling air increased more sharply with pressure at a temperature of 680 °C, and the accompanying decrease in efficiency was more severe. However, at 95 wt%, the curves in Fig. 9B for 680 °C and 850 °C are very close because the methane reforming or methanation reactions are negligible at higher moisture contents, and therefore the effects described at 80 wt% are not apparent at 95 wt%.

The maximum efficiency of the SCWG-rSOC system in FC mode was found to be 66 % at the following conditions:

rSOC pressure of 1 bar.

moisture content of 80 wt%.

rSOC temperature of 850 °C.

At 95 wt% and 1 bar, the efficiency decreased to 56 % at 680 °C and 54 % at 850 °C.

15. Effect of current density on the efficiency of the SCWG–rSOC system in FC mode

Fig. 9B and Fig. 9C illustrate the effect of current density (*j*) on the SCWG–rSOC system energy efficiency in FC mode at 95 and 80 wt% biomass moistures, respectively, at varying rSOC operating pressures and temperatures. Two different situations were evaluated for the rSOC in FC mode: a) fresh syngas as fuel, and b) mixed syngas as fuel. While the current density was varied, the fuel flowrate and the stack area were constant. Therefore, fuel utilisation factor also increased proportionally with current density. However, due to the different flow rates of fresh and mixed syngas, the achievable current densities for those two cases was very different. In order to make a proper comparison between the trends in the same figure, the X-axes of Fig. 9B and 9C use the current density between the minimum and maximum current densities for each case in the figure.

At 95 wt% biomass moisture, and rSOC pressure of 1 bar, and rSOC temperature of 850 °C, the power generated by the rSOC fed by fresh syngas was 7.2 kW. However, the rSOC power increased to 86.25 kW when the mixed syngas was fed to the rSOC. This was due to the higher flow rate and calorific value of the mixed syngas.

At a higher temperature (850 °C) and lower pressure (1 bar), the system efficiency monotonically increased with increasing *j*. At higher *j* values, a greater portion of the fuel was consumed in the stack.

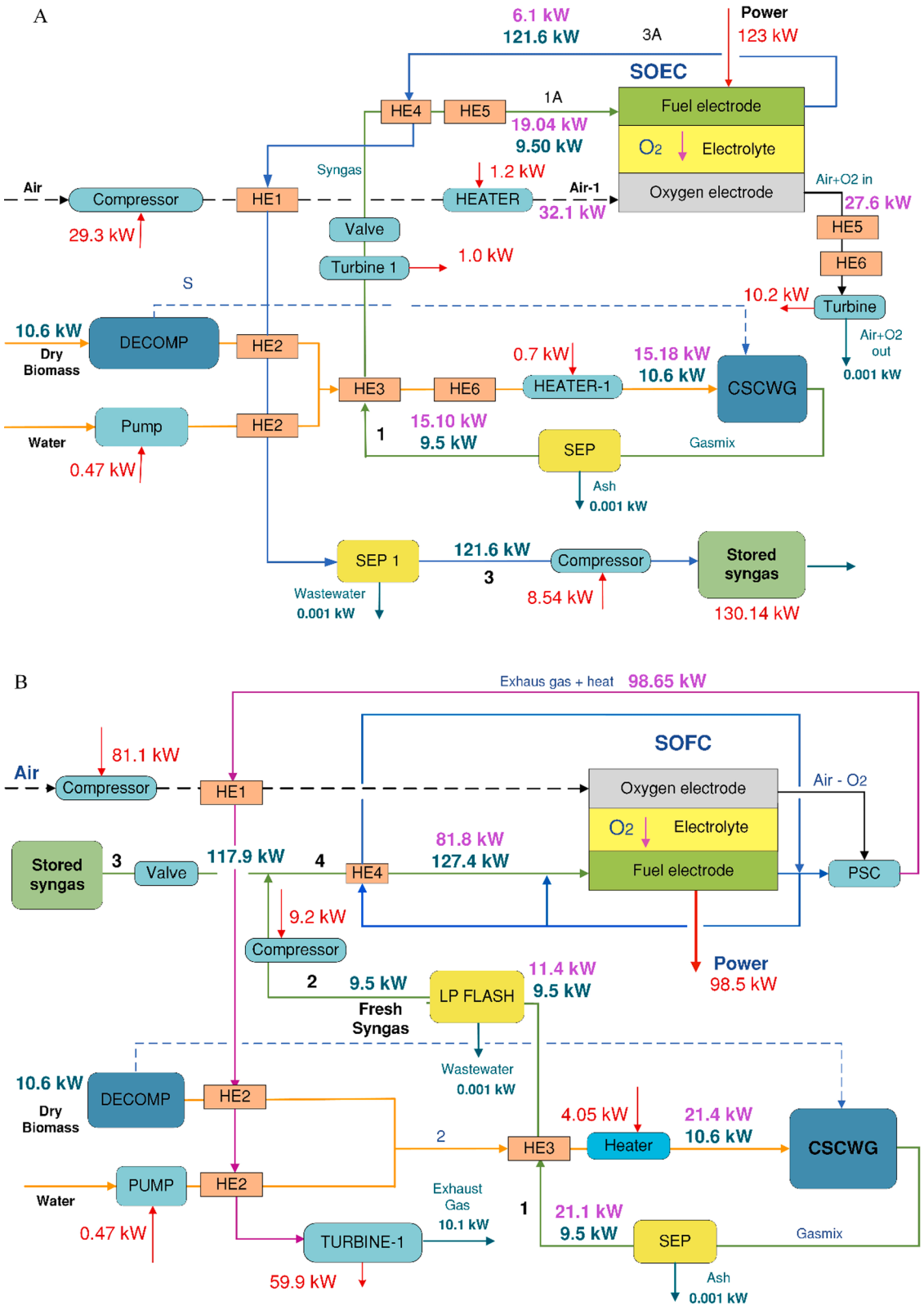

Fig. 7. Flowsheet of the SCWG–rSOC system at j = 3.4 A cm^{-2}, T = 680 °C, P = 20 bar, biomass moisture content = 95 wt%. The figures include electricity consumption and production (red), as well as chemical exergy flows (green), thermochemical exergy flow (pink). Stream numbers refer to Table 5 with gas compositions. A) SCWG–rSOC – EL. B) SCWG–rSOC – FC. C) SCWG–SOFC.

Therefore, stack power output increased, while the PSC had to burn less fuel. Lower fuel combustion in the PSC led to smaller combustion losses and lower exhaust gas temperatures. Lower exhaust gas temperatures, in turn, led to a lower fuel temperature at the HE1/HE2 outlets (in Fig. 2B). Therefore, HE3 recovered more heat from the gasifier outlet, and less heat was lost in the gas/liquid separator (LPFLASH). The lower exhaust

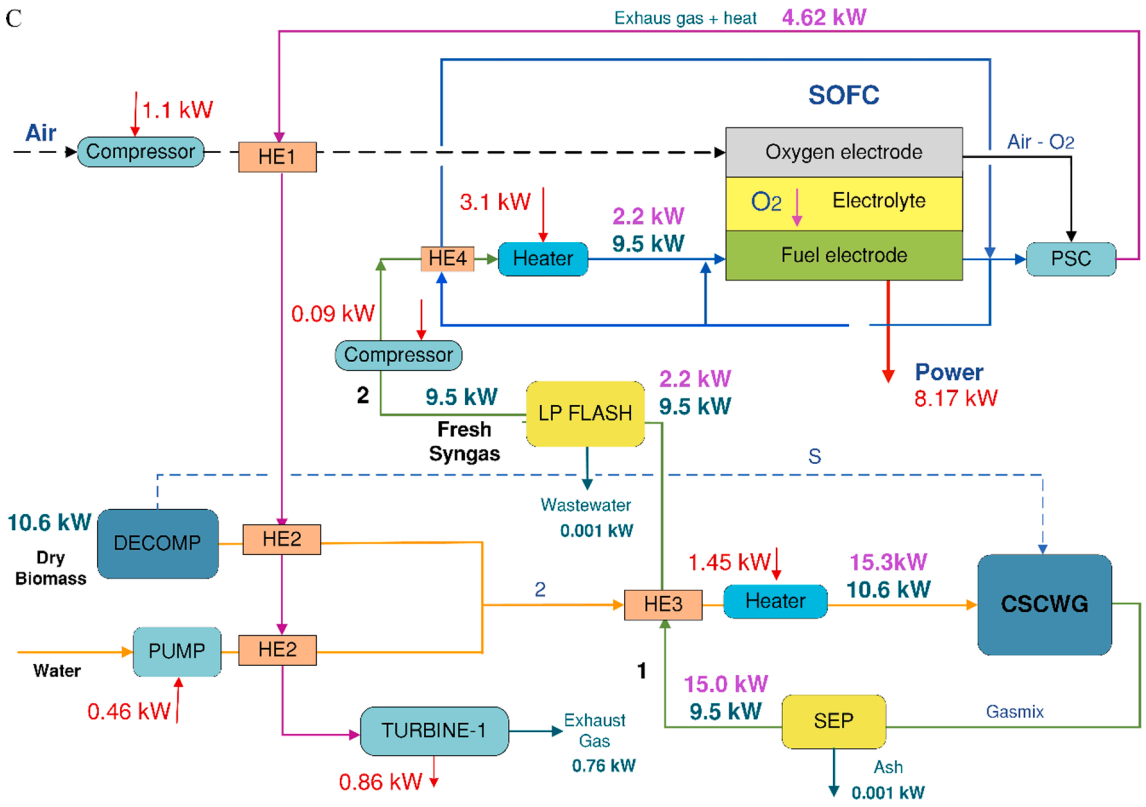

Fig. 7. (*continued*).

gas temperatures also led to more efficient heat transfer with the incoming air and fuel due to the smaller temperature differences in the heat exchangers (HE1/HE2/HE4). All these factors led to higher efficiency at higher j values. On the other hand, at lower j values, the PSC had to combust more fuel and additional air was supplied to limit the gas temperature to<1000 °C. The additional heat generated in the PSC was lost to the environment via exhaust gas and LPFLASH, leading to lower efficiency.

At 95 wt% moisture, the current density was only between 0.12 and 0.14 A·cm^{-2} when fresh syngas was used. The maximum system efficiency is not reached at 850 °C and 1 bar at current density < 0.14 A·cm^{-2}, contrary to at 680 °C and 20 bar. By contrast, the current density varied between 1.2 and 1.7 A·cm^{-2} when mixed syngas was used. Therefore, more heat was generated in the rSOC with mixed syngas due to the higher fuel consumption and higher overpotentials. This excess heat was lost through the air exhaust and the liquid/gas separator.

However, at a lower temperature (680 °C) and higher pressure (20 bar), the system efficiency reached its maximum at $j \approx 1.5$ A·cm^{-2} and then decreased with further increase in j. At $j < 1.5$ A·cm^{-2}, an increase in j improved efficiency for the same reasons stated in the previous paragraphs. But at $j < 1.5$ A·cm^{-2}, the rSOC became highly exothermic owing to the higher fuel consumption and current overpotentials. Therefore, the required cooling airflow and air compressor power grew very large, reducing the efficiency despite the other benefits mentioned above. The maximum system efficiency depend on the fuel utilization and thus the current density [68].

The trends for lower biomass moisture content (80 wt%), Fig. 6C, were similar to those for higher biomass moisture content as discussed above, but the efficiencies were higher at lower moisture contents. This occurred for several reasons:

The syngas flow rate was lower at lower moisture contents, leading to decreased heat generation in the rSOC and smaller heat losses to the environment, as mentioned above;

The lower moisture and the accompanying lower biomass flow rate meant that the gasifier required less external heat for preheating and for driving the reactions in the gasifier.

The higher content of CH_4 in the flow promotes endothermic side reaction such as CH_4 reforming, thus reducing the energy utilized for heat removal by the air compressor.

These effects resulted in a higher efficiency at a lower biomass moisture content.

16. Sensitivity analysis of SCWG-rSOC EL operation

16.1. Effect of rSOC pressure and temperature on the efficiency of the SCWG–rSOC system

Fig. 10A illustrates the influence of the operating pressure and temperature of the rSOC on the SCWG–rSOC system in EL mode at 95 wt % biomass moisture content.

At rSOC temperature of 680 °C, the rSOC was exothermic; therefore, the cooling airflow was relatively small. In this situation, increasing the rSOC pressure improved the system efficiency, from 87 % at 1 bar, to 90 % at 20 bar. At higher pressures, there was a significant increase in the temperature of fuel and air in the compressors. This greatly reduced the external heat demand for preheating. Further, higher pressure increased the rSOC voltage (due to increase in the Nernst voltage), making the stack more exothermic. This heat was used to preheat the air and fuel, further decreasing the external heat requirement. The stack power and air compressor power also increased at higher pressure, but the decrease in external heat requirement was more significant, increasing the overall system efficiency at higher pressures. The efficiency slightly increases after 13 bar, then stabilizes at 20 bar, obtaining the highest efficiency of 90 %. Therefore, the calculation was made at 20 bar in the subsequent results. The system could also work optimally at pressures between 13 and 14 bar to reduce engineering limitations for practical application in future research.

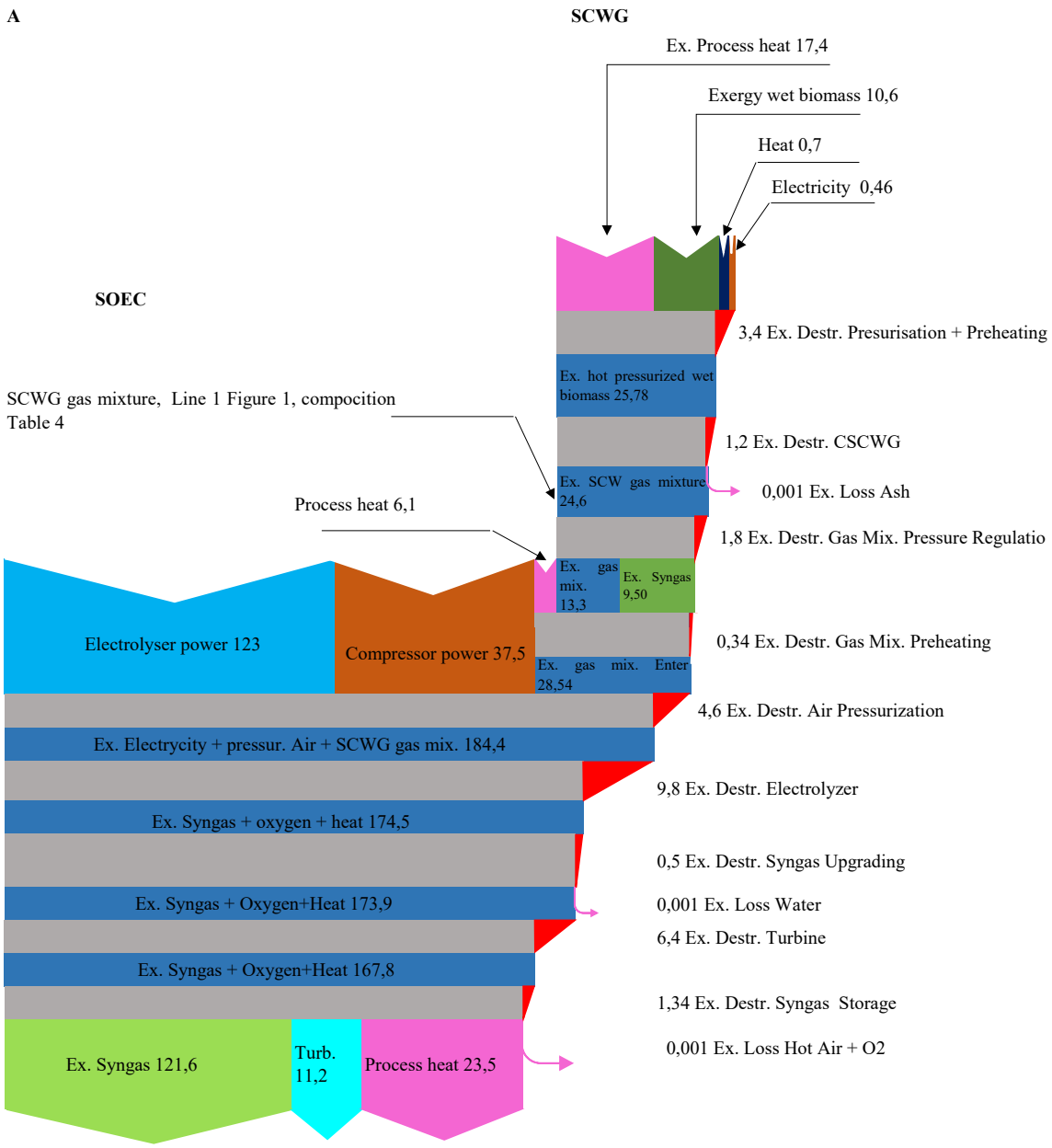

Fig. 8. Exergy flow diagram (kW) of the SCWG–rSOC system at $j = 3.4$ A cm^{-2}, $T = 680$ °C, $P = 20$ bar, biomass moisture content = 95 wt%. A) SCWG- rSOC EL mode, B) SCWG- rSOC FC mode with mixed syngas, and C) SCWG–rSOC FC mode with fresh syngas.

At rSOC temperature of 750 °C, the rSOC was endothermic. The air flow required to provide this heat was also high. Therefore, the air compression power increased sharply as the pressure was increased. The stack power also increased at higher pressure, due to the increased Nernst voltage. Due to the high temperature and endothermic nature of the stack, a large amount of external heat was required to preheat the air and fuel. This heat demand decreased at higher pressures, just as mentioned before, but the increase in stack power and air compressor power were much more significant in this case, due to the higher air flow rate. Therefore, the system efficiency greatly decreased with increased pressure, from 88 % at 1 bar to 81 % at 20 bar.

At rSOC temperature of 850 °C, the rSOC is more endothermic than at 750 °C, and therefore the airflow required to heat the stack is much higher. Therefore, the decrease in efficiency with pressure is much sharper at 850 °C due to the greater influence of air compressor power. Similarly, at 550 °C, the rSOC is more exothermic than at 680 °C and the cooling airflow is higher than at 680 °C. Therefore, the improvement in efficiency with increased pressure is lower at 550 °C, due to the greater influence of air compressor power.

In all these cases, higher pressure increases the exothermic methanation in the stack. However, because the biomass has 95 % moisture, the amount of methanation is small, and these changes are not very significant compared to the other changes in BoP power and heat demand.

Notably, the thermal efficiency of biofuel production by SCWG–rSOC achieved with this approach overcomes the previously determined production efficiency limit of 45 % for thermochemical biomass gasification plus steam electrolysis and of 30 % for solar–electrochemical hydrogen [8,69].

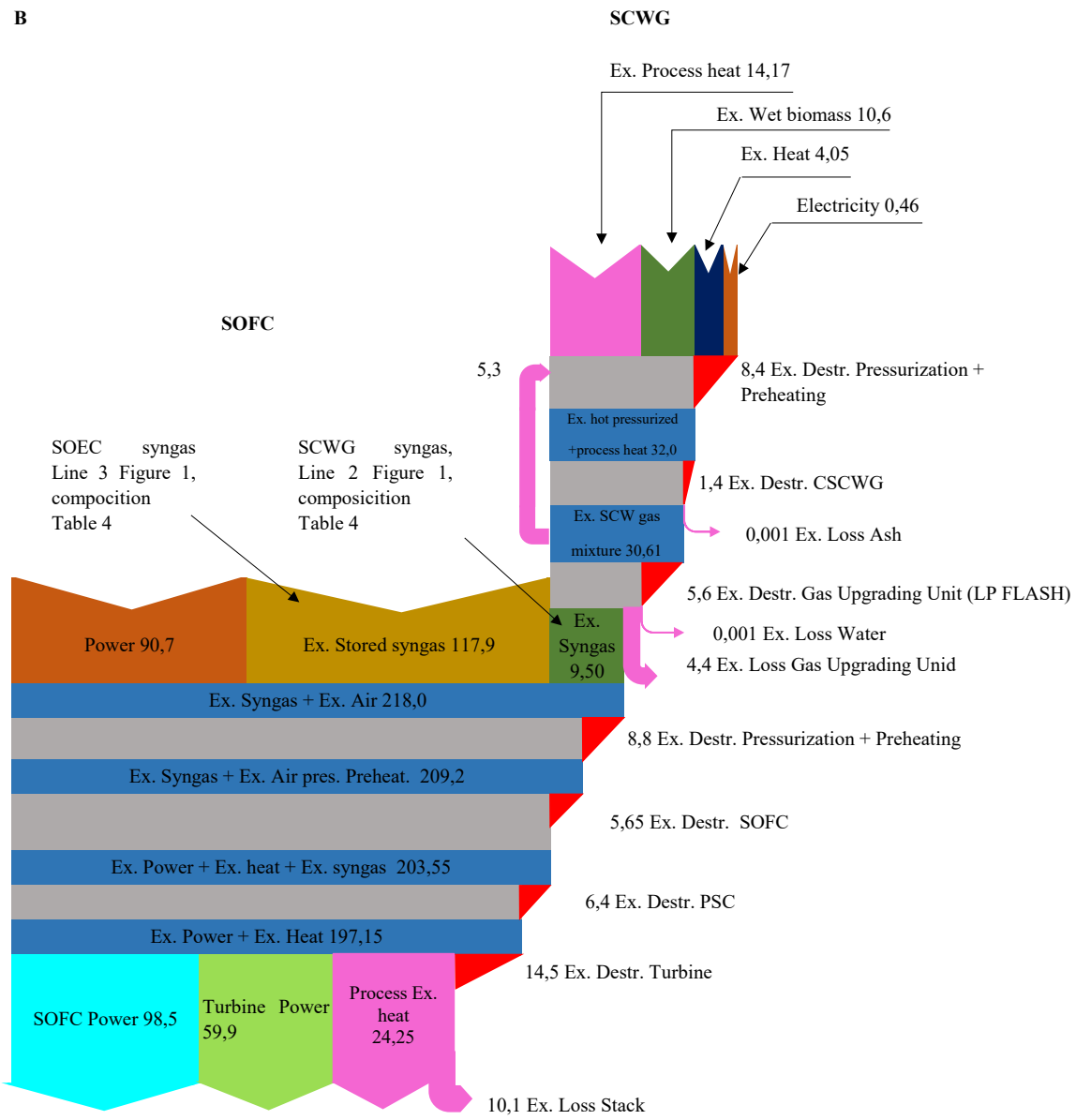

Fig. 8. (*continued*).

17. Effect of current density on the efficiency of the SCWG–rSOC system in EL mode

Fig. 10B shows the variation of system energy efficiency with rSOC current density, for different biomass moisture contents. At each level of moisture, the flow rates of biomass had significant variations. This was because the dry biomass flow was held constant at 0.56 g/s, while the water flow rate (as part of the wet biomass) was changed as needed, from 2.24 g/s at 80 wt% to 10.64 g/s at 95 wt%. Because of this, if the rSOC active area would be held constant, then the current densities would vary too far away from the optimum efficiency values. Therefore, a different rSOC area had to be considered for each moisture level, to avoid excessively low or high current densities, thus maximising efficiencies. At 95 wt%, this area was 2.624 m^2, and at 80 wt%, it was 0.525 m^2.

At a 95 wt% moisture content, the optimal current density was 3.4 A cm^{-2}, at which value the system reached a maximum energy efficiency of 91 %. When the SOEC was operated at a lower moisture content, i.e., 80 wt%, the maximum energy efficiency decreased to 86 %, achieved at 2.9 A cm^{-2}. To electrochemically reduce H_2O at 95 wt% moisture content, the rSOC required a higher current density and heat than at a lower moisture content owing to the larger flow rate. Maximum system efficiency was reached at a cell voltage (1.32 V) slightly greater than the thermoneutral voltage (approx. 1.26 V). The increased current density makes the rSOC system exothermic, which favours the highest system efficiency due to the use of this generated heat to meet the air and fuel preheating demand.

At a higher moisture content, the concentration of syngas produced in the SCWG was 5 % of the gaseous mixture, which contained H_2, CH_4, CO, and CO_2, promoting the exothermic methanation reaction to some extent. However, at a lower moisture content, i.e., 80 wt%, the mixture processed by the rSOC contained a larger proportion of syngas, which constituted approximately 20 % of the gaseous mixture. This increased methanation, leading to additional heat generation, making the stack highly exothermic. This additional generated heat provided for the heat requirements of the system. However, the power required to compress more air to remove the heat under exothermic operation had a greater negative effect on the system efficiency. Therefore, the peak efficiency at 80 wt% moisture content was lower than at 95 wt%.

The airflow rate and air inlet temperature (oxygen electrode) can be

C

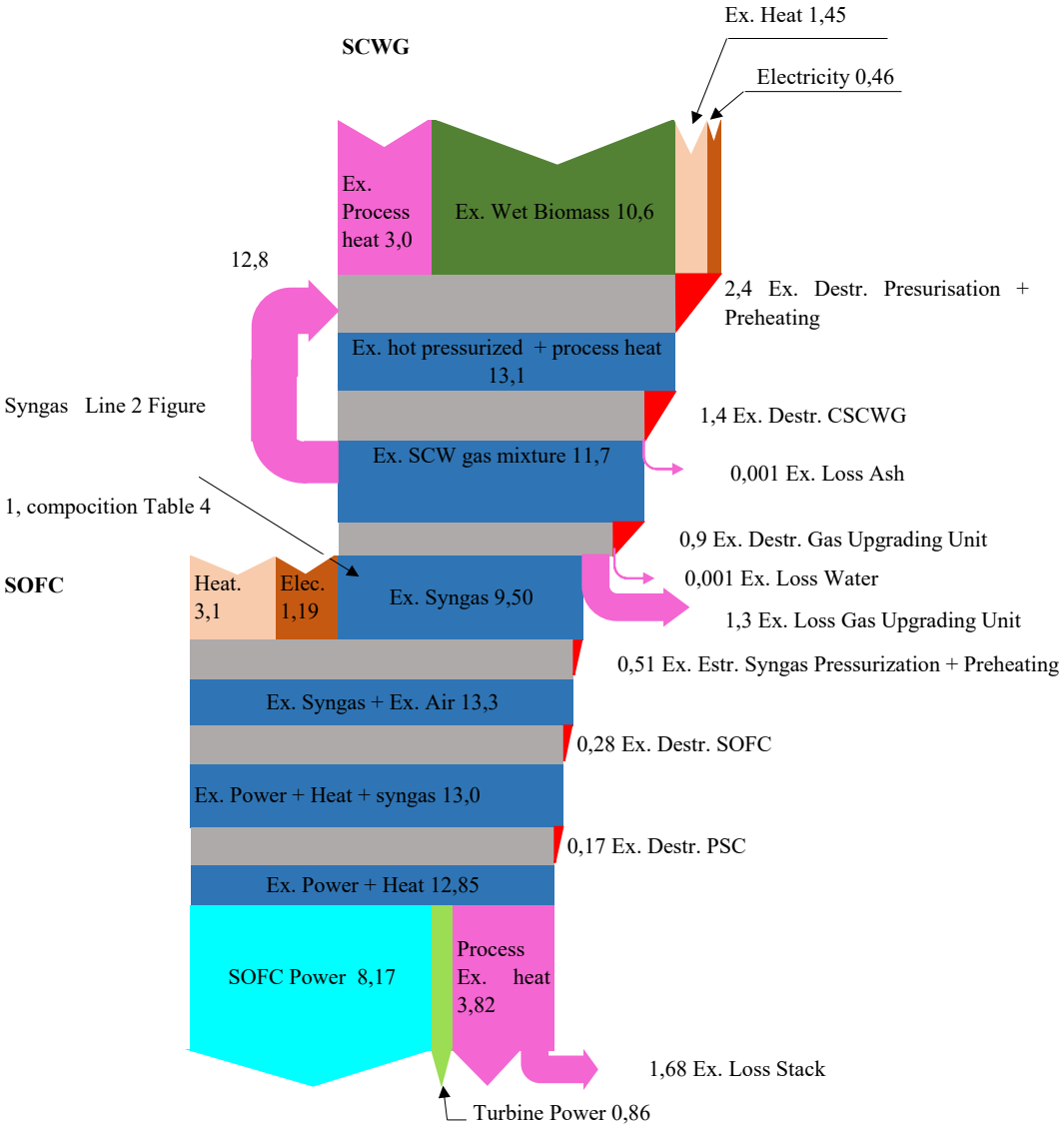

Fig. 8. (*continued*).

changed to extract or provide heat to the stack. The heat from the rSOC air electrode exhaust provided the heat for air and fuel preheating, as well as for the SCWG. The heat available from the stack was 4.7 kW at 95 wt% moisture, and 1.5 kW at 80 wt%. The power supplied to the compressor at 95 wt% was 19 % of the total power input, whereas it was 37 % at 80 wt%. The turbines recovered a significant amount of waste heat in the form of electricity, to the tune of 7.4 kW and 2.6 kW, at 95 wt % and 80 wt%, respectively. At the thermoneutral voltage, the least power was required to drive the compressor, but the external heat required by the system BoP to preheat the air and fuel was high, which reduced the efficiency. On the other hand, at the optimum voltage (slightly above thermoneutral voltage), the compressor power was higher, but the external heat requirements were very low, thus maximising the efficiency.

Any increase in the current density from the optimal value made the rSOC highly exothermic, causing it to generate excess heat that was removed by the airstream. This in turn increased the power required to drive the air compressor, and consequently reduced the system efficiency. However, at a current density lower than optimum, the rSOC exhibited endothermic behaviour. The airstream supplemented the heat demand of the system by increasing the inlet air flow rate and inlet temperature. Thus, the external heat provided the heat requirements of the electrolyser through the airflow, and the air compressor consumed more power, reducing the system efficiency.

18. The efficiency of the SCWG–rSOC system

Fig. 10C shows the system efficiencies of the SCWG–rSOC system at 95 wt% biomass moisture content as a function of the current density *j* of the rSOC, in both modes. The system efficiency in FC mode was higher at lower current densities, whereas the system efficiency in EL mode was higher at higher current densities. The rSOC can operate at different current densities in both modes [70].

The operation of the reversible system with an active area of 3.375 m^2 in a similar current density range (2–3 $A{\cdot}cm^{-2}$) in both modes. The rSOC in FC mode, operating at high current densities saw an increment in the generated heat, reducing the efficiency. In EL mode, within the range under consideration, the efficiency increases with current density due to operation moving closer to thermoneutral point. The FC mode efficiency was around 40–45 % whereas the EL mode efficiency was

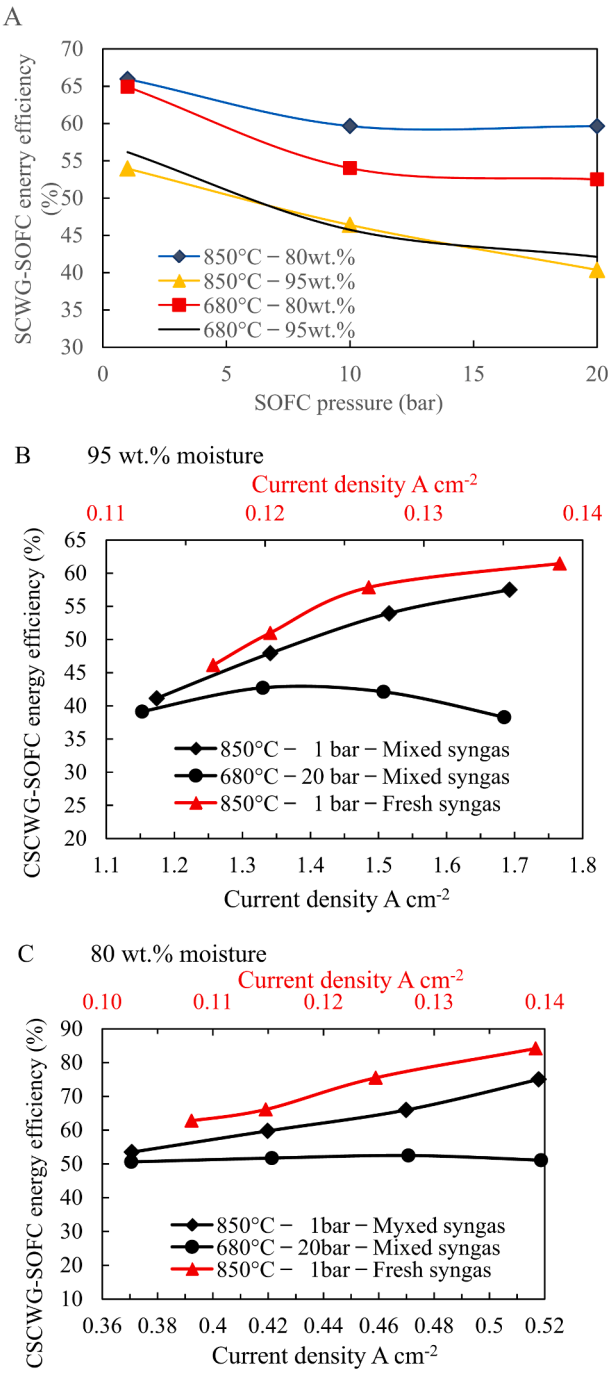

Fig. 9. A) Effect of SOFC pressure and temperature on the SCWG-rSOC FC mode system's efficiency. B) Effect of current density on the SCWG-rSOC FC mode efficiency at different pressures, temperatures, and fuel flow rates (SCWG–stored syngas, and SCWG syngas) at 80 wt% and C) 95 wt% biomass moisture content.

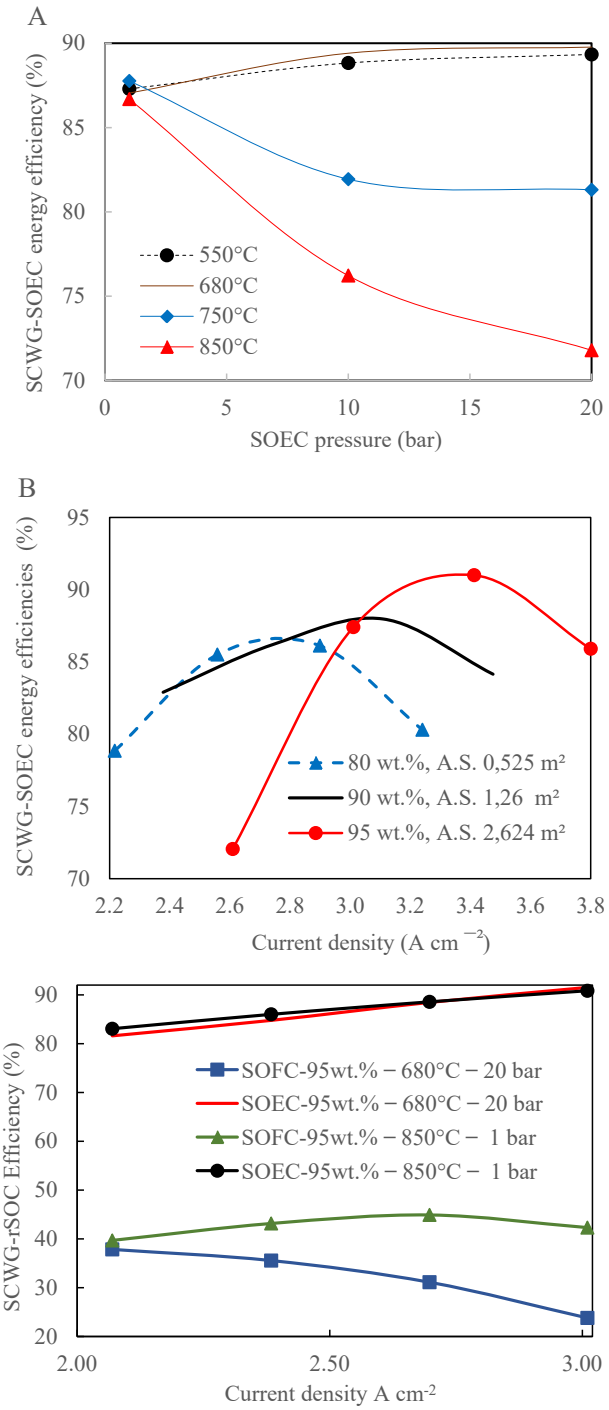

Fig. 10. A) Effect of rSOC operating pressure and temperature on the SCWG–SOEC energy efficiency at 95 wt% biomass moisture content. B) Effect of the current density on the SCWG–SOEC system energy efficiency at 680 °C and 20 bar. C) A comparison of the effect of current density on both operating modes.

around 80–90 %. The efficiency of biomass gasification and reversible solid-oxide cell stack reaches 50 %-60 % for power generation, 72 %-76 % for power storage mode is presented in the findings of [71].

19. Exergy destruction in the SCWG-rSOC system

Fig. 11A illustrates the contribution of each process unit to the total exergy destruction of the SCWG-rSOC system in EL mode, for different biomass moisture contents at the highest system efficiencies from Fig. 10B. The total exergy destruction increased with the biomass moisture content because of the increased exergy available. The most significant contributions to exergy destruction were from the rSOC, turbines, and preheating for rSOC reactants. The SCWG, preheating for SCWG reactants, and SEP exhibited lower exergy destruction rates. The exergy destruction due to chemical reactions was the largest component of exergy destruction in the rSOC-EL mode, increasing from 0.22 kW at 80 wt% to 0.35 kW at 95 wt%. A high biomass moisture content facilitated more chemical and electrochemical reactions in the rSOC owing to

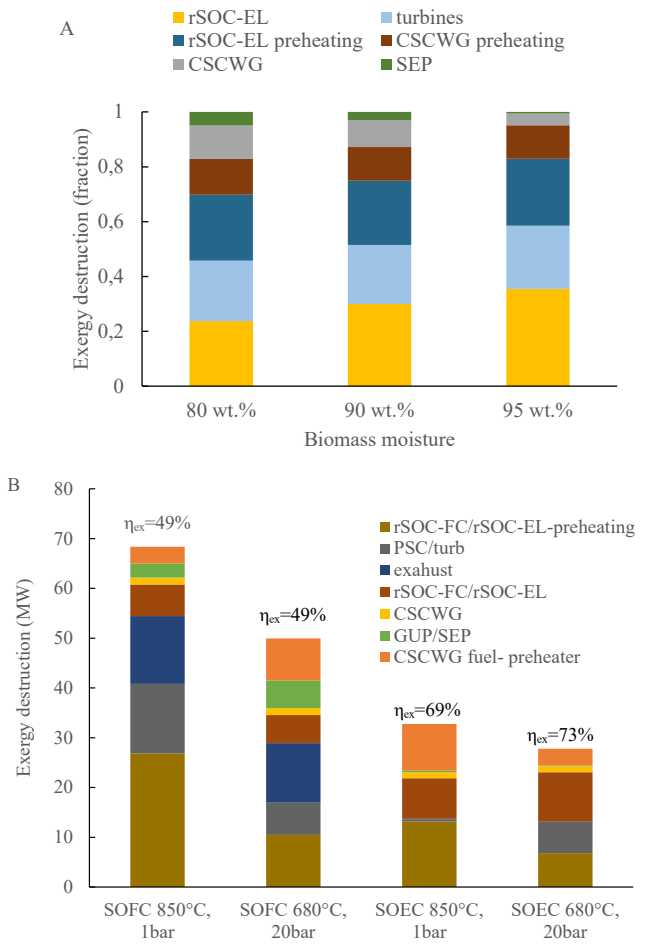

Fig. 11. Contribution of process unit exergy destruction to the total exergy destruction. A) rSOC operation in EL mode as a function of biomass moisture content at 20 bar, 680 °C, j = 2.9, 3.1 and 3.4 A cm^{-2} at 80, 90 and 95 wt% moisture contents. B) FC and EL mode operation, biomass moisture content = 95 wt%, 20 bar, 680 °C, FC j = 1.5 A cm^{-2}, EL j = 3.4 A cm^{-2} and 1 bar, 850 °C, FC j = 1.5 A cm^{-2}, EL j = 3.4 A cm^{-2}.

the higher water content, which led to a greater exergy destruction. The exergy destruction in preheating of rSOC reactants was caused by the significant temperature differences between the streams in the heat exchangers, considering that air and biomass entered the system at ambient pressure and temperature, and the hot streams had a temperature as high as 680 °C. Exploring more efficient energy recovery pathways could therefore represent a promising topic for future studies. The exergy destruction of the SEP and SCWG reduced with moisture is remarkable. High water content determines gasification [29,30].

Fig. 11B describes the exergy destruction in each process unit of the SCWG-rSOC system in reversible operation at various operating conditions. At 680 °C and 20 bar, the exergy efficiencies were 49 % and 73 % in the FC and EL mode, respectively. Variations in the operating pressure and temperature of the rSOC influenced the heat and power required by the system. The air and fuel preheating in the rSOC exhibited higher exergy destruction because of high temperature differences in the heat exchanger units. At a lower temperature and high pressure, the pressurised air and fuel required less process heat for preheating. Thus, the exergy destruction in heat exchangers was reduced. The exergy destruction in SEP is almost negligible due to the small fraction of separated water, unlike in GUP. Table 6 reports the key data describing the system performance.

20. Conclusions and future outlook

This study investigated a process design for a combined SCWG-rSOC system, which can attain high efficiencies in energy conversion and has a high capacity for hydrogen production. By doing so, three needs have been met effectively: sustainable sanitation, biofuel and power generation from waste, and renewable energy storage. As a standalone unit, SCWG using high moisture biomass produces syngas with high steam and CO_2 content. This system overcomes this limitation by converting the steam and CO_2 into more syngas. The integration of SCWG and rSOC technology represents a new approach that – together with improvements in materials, residence time, and stable catalysts at a competitive price – will help commercialise SCWG-rSOC technology.

The SCWG–rSOC system exhibited high performance at a biomass moisture content of 95 wt%. At rSOC operating conditions of 680 °C and 20 bar, syngas production with the system in EL mode achieved energy and exergy efficiencies of 89 % and 73 %, respectively. The use of an rSOC (in EL mode) increased the yield of syngas by approximately thirteen times compared to that produced exclusively by the SCWG. The SCWG syngas production exergy efficiency reported in the literature at biomass moisture > 90 wt% is around 20 %. The total exergy destruction of the SCWG-EL mode is comprised of the following parts: exergy destruction in the electrolyser, heat exchange process, and turbines. The exergy destruction of gas/liquid separator is negligible. SOEC operation at high pressure and lower temperature result in lower total exergy destruction. Higher feedstock moisture increases the exergy destruction, but the utilisable exergy increases. The system efficiency reached a maximum of 91 % at a current density of 3.4 A cm^{-2}.

The high-quality syngas produced in EL mode was stored in a tank and then used in FC mode along with freshly produced syngas from the SCWG. This increased the power output in the FC mode by a factor of twelve, compared to the use of syngas produced solely by the SCWG. The system in FC mode achieved energy and exergy efficiencies of only 42 % and 49 %, respectively.

However, the proposed SCWG–rSOC energy storage system is currently subject to limitations that may prevent its use for large-scale power generation. First, in the rSOC field, a new system configuration for the SCWG–rSOC must be identified to reduce the mentioned exergy destruction and losses. Second, since the presence of CH_4 has a significant influence on the thermal behaviour of the rSOC, it is necessary to gain a better understanding of the chemical and electrochemical behaviour of CH_4 under fuel utilisation to improve the SCWG–rSOC performance.

The proposed technology has been shown to efficiently generate fuel or power. Manure, sewage, industrial waste, agriculture waste, or algae, can be used to feed the proposed system. As the increasing global population requires high quality water and air to ensure the health of all living species, increased efforts to develop sustainable methods for energy generation and sanitation provision are urgently required over the next decade(s); the proposed SCWG–rSOC system is a step in this direction.

CRediT authorship contribution statement

Mayra Recalde: Conceptualization, Methodology, Writing – original draft. **Amogh Amladi:** Data curation, Writing – review & editing, Validation. **Vikrant Venkataraman:** Writing – review & editing. **Theo Woudstra:** Validation. **Purushothaman Vellayani Aravind:** Supervision.

Declaration of Competing Interest

The authors declare that they have no known competing financial interests or personal relationships that could have appeared to influence the work reported in this paper.

Data availability

Data will be made available on request.

Acknowledgment

This study was conducted under financial support the Ecuadorian Institution, Secretaría de Educación Superior, Ciencia, Tecnología e Innovación (SENESCY) by the PhD scholarship. We thank Giulia Botta and Alvaro Fernandes (TUDelft) for their collaboration in fuel cell modelling.

Appendix A

The Ohmic overpotential occurs due to the electrolyte resistance to the ionic current O^{-2}. The resistance include the solid electrolyte and the electrodes. In this work, it is assumed the electrode resistance are negligible. The Ohmic losses depend on the cell design, electrolyte thickness and material. They depend on the ionic and electronic conductivity σ_{el} [$\Omega^{-1}m^{-1}$] of the electrolyte [24]:

$$\eta_{ohm} = j \bullet \frac{\delta_{el}}{\sigma_{el}} \tag{17}$$

Where δ_{el} is the electrolyte layer thickness, $r_{ohm,el}$ is the specific Ohmic resistance of the electrolyte layer [Ωcm^2] and $r_{Ohmic,const}$ is the resistance of interconnectors and wires [Ωcm^2], which is assumed to be constant. On the other hand, the electrolyte conductivity σ_{el} strongly depends on temperature and can be calculated as [72]:

$$\sigma_{el} = \sigma_{0,el} T^{-1} \bullet exp\left(-\frac{E_{el}}{R \bullet T}\right) \tag{18}$$

where $\sigma_{0,el}$ [$\Omega^{-1}m^{-1}$] is an empirical pre-exponential factor, and E_{el} [J/mol] is the activation energy.

Concentration/Diffusion overpotential. During cell operation, the reactant and product are transported by diffusion through the porous media from the bulk of material to the TPB or vice versa. The geometrical effects and molecular interactions generate diffusion losses that result in lower reactant and product partial pressure at the TPB. Assuming the system contain binary components, the concentration losses according to [42] result:

$$\eta_{conc,fuel} = \frac{R \bullet T}{2 \bullet F} \bullet ln\left(\frac{p_{H_2O,tpb} \bullet p_{H_2,bulk}}{p_{H_2O,bulk} \bullet p_{H_2,tpb}}\right) \tag{19}$$

$$\eta_{conc,oxygen} = \frac{R \bullet T}{4 \bullet F} \bullet ln\frac{p_{O_2,bulk}}{p_{O_2,tpb}} \tag{20}$$

where $p_{i,bulk}$ and $p_{i,tpb}$ are respectively the bulk and TPB gas concentration as a function of the partial pressure of the species i in a binary mixture i and j. According to Fick's model, the gas concentration is given by [42]:

$$p_{i,tpb} = p_{i,bulk} - \frac{R \bullet T \bullet \delta_{an,cat}}{n_i \bullet F \bullet D_{eff,i}} \tag{21}$$

considering that Knudsen diffusion and molecular diffusion compete with one another, the effective diffusion coefficient $D_{eff,i}$ [m^2/s] is determined by [42]:

$$D_{eff,i} = \frac{\varepsilon}{\tau} \bullet \left(\frac{1}{D_{ij}} + \frac{1}{D_{ik}}\right) \tag{22}$$

where the path for the diffusion of the gas molecules within the pores has a tortuosity τ and average pore diameter ε. The pure Knudsen diffusion comprises the effect of the porous medium and is estimated by [42]:

$$D_{ik} = \frac{d_p}{3}\sqrt{\frac{8RT}{\pi M_i}} \tag{23}$$

where M_i is the molecular weights of gas species i, and d_p is the mean pore size of the porous media. The binary diffusivity coefficient D_{ij} is given by [42]:

$$D_{ij} = \frac{1.43 \bullet 10^{-7} \bullet T^{1.75}}{p \bullet \sqrt{2/\left(M_i^{-1} + M_j^{-1}\right)}\left(V_{d,i}^{1/3} + V_{d,j}^{1/3}\right)^2} \tag{24}$$

where V_d is the atomic diffusion volumes of species i and j.

Activation losses. The charge-transfer resistance depends on the TPB area and operating conditions such as gas composition and temperature. The inverted Butler-Volmer [54] Eqs. 26 and 29 compute the charge-transfer activation overpotentials ($\eta_{act,a}$ $\eta_{act,c}$). In the present work is assumed that only the oxidation of H_2 takes place in the TPB, and the charge-transfer reaction at the TPB region is the limiting step in the anode and cathode. The limiting step reaction of electrochemical oxidation of H_2 is giving by Eq. 25, [52].

$$H_{(Ni)} + OH^-_{(YSZ)} \leftrightarrow (Ni) + H_2O_{(YSZ)} + e^-_{Ni} \tag{25}$$

$$\eta^a_{act} = \frac{RT}{F}\left[sinh^{-1}\left(\frac{i}{2i_{0,anode}}\right)\right] \tag{26}$$

where i_0 is the exchange current density:

$$i_0 = i^*_{H_2} \frac{\left(p_{H_2}/p^*_{H_2}\right)^{1/4}\left(p_{H_2O}\right)^{3/4}}{1+\left(p_{H_2}/p^*_{H_2}\right)^{1/2}} \tag{27}$$

The balance between adsorption and desorption of hydrogen on the Ni determines the parameter $p^*_{H_2}$. According to [52] there are not yet established values for the forward and reverse rates of hydrogen adsorption and desorption on Ni, and they are a function of different variables such as the particular crystal face and surface defects. In the work of [52] the dissociative adsorption rate is written in terms of a sticking probability γ_0. Table 1A shows the parameters.

$$p^*_{H_2} = \frac{A_{des}\Gamma^2\sqrt{2\pi \mathrm{R}\mathrm{T}M_{H_2}}}{\gamma_0} exp\left(\frac{E_{des}}{RT}\right) \tag{28}$$

$i^*_{H_2}$ depends on parameters associated with the charge-transfer reactions. However, parameters like the specific three-phase boundary length and the elementary charge-transfer rates are not directly known. Thus, here we take $i^*_{H_2}$ as a fitting value.

Eq. 29 describes the electrochemical reduction of oxygen incorporated at the electrode–electrolyte interface [54]:

$$\eta^c_{act} = \frac{RT}{F}\left[sinh^{-1}\left(\frac{i}{2i_{0,cathode}}\right)\right] \tag{29}$$

The charge transfer and incorporation at the TPB [54]:

$$O_{ad(c)} + V_{\ddot{O}(el)} + 2e^-_{(c)} \leftrightarrow O^{\times}_{O}(el) + (c) \tag{30}$$

$O_{ad(c)}$ is adsorbed atomic oxygen on the cathode surface and (c) is an unoccupied cathode surface site, $V_{\ddot{O}(el)}$ is the oxide-ion vacancy and $O^{\times}_{O}(el)$ is an oxide anion. i_0 is the exchange current density:

$$i_0 = i^*_{O_2} \frac{\left(p_{O_2}/p^*_{O_2}\right)^{1/4}}{1+\left(p_{O_2}/p^*_{O_2}\right)^{1/2}} \tag{31}$$

$i^*_{O_2}$ is a fitting parameter, see Table 1A for parameters.A_{O_2}, E_{O_2}

$$p^*_{O_2} = A_{O_2}\exp\left(-\frac{E_{O_2}}{RT}\right) \tag{32}$$

References

[1] IEA, World Energy Outlook 2018 - Scenarios, 2018.
[2] BP, BP Energy outlook 2017, BP Stat. Rev. World Energy. (2017) 52. https://doi.org/10.1017/CBO9781107415324.004.
[3] International Energy Agency, Renewables 2020, Int. Energy Agency. (2020).
[4] UNEP, Water Quality: Policy Brief, Unwater. (2011).
[5] UNICEF, The Impact of Poor Sanitation on Nutrition, 2014.
[6] Damo UM, Ferrari ML, Turan A, Massardo AF. Solid oxide fuel cell hybrid system: A detailed review of an environmentally clean and efficient source of energy. Energy 2019;168:235–46.
[7] sunfire, (n.d.). https://www.sunfire.de/en/hydrogen.
[8] Sigurjonsson HÆ, Clausen LR. Solution for the future smart energy system: A polygeneration plant based on reversible solid oxide cells and biomass gasification producing either electrofuel or power. Appl Energy 2018;216:323–37.
[9] Clausen LR, Butera G, Jensen SH. High efficiency SNG production from biomass and electricity by integrating gasification with pressurized solid oxide electrolysis cells. Energy 2019;172:1117–31.
[10] Anghilante R, Müller C, Schmid M, Colomar D, Ortloff F, Spörl R, et al. Innovative power-to-gas plant concepts for upgrading of gasification bio-syngas through steam electrolysis and catalytic methanation. Energy Convers Manag 2019;183:462–73.
[11] Ali S, Sørensen K, Nielsen MP. Modeling a novel combined solid oxide electrolysis cell (SOEC) - Biomass gasification renewable methanol production system. Renew Energy 2020;154:1025–34.
[12] Xu Y-P, Lin Z-H, Ma T-X, She C, Xing S-M, Qi L-Y, et al. Optimization of a biomass-driven Rankine cycle integrated with multi-effect desalination, and solid oxide electrolyzer for power, hydrogen, and freshwater production. Desalination 2022;525:115486.
[13] Habibollahzade A, Gholamian E, Behzadi A. Multi-objective optimization and comparative performance analysis of hybrid biomass-based solid oxide fuel cell/solid oxide electrolyzer cell/gas turbine using different gasification agents. Appl Energy 2019;233-234:985–1002.
[14] Erlach B, Harder B, Tsatsaronis G. Combined hydrothermal carbonization and gasification of biomass with carbon capture. Energy 2012;45(1):329–38.
[15] van Wyk S, van der Ham AGJ, Kersten SRA. Potential of supercritical water desalination (SCWD) as zero liquid discharge (ZLD) technology. Desalination 2020;495:114593.
[16] Hodes M, Marrone PA, Hong GT, Smith KA, Tester JW. Salt precipitation and scale control in supercritical water oxidation - Part A: Fundamentals and research. J Supercrit Fluids 2004;29(3):265–88.
[17] Timko MT, Ghoniem AF, Green WH. Upgrading and desulfurization of heavy oils by supercritical water. J Supercrit Fluids 2015;96:114–23. https://doi.org/10.1016/j.supflu.2014.09.015.
[18] Boukis N, Hauer E, Herbig S, Sauer J, Vogel F. Catalytic gasification of digestate sludge in supercritical water on the pilot plant scale. Biomass Convers Biorefinery 2017;7:415–24. https://doi.org/10.1007/s13399-017-0238-x.
[19] Antal MJ, Allen SG, Schulman D, Xu X, Divilio RJ. Biomass Gasification in Supercritical Water †. Ind Eng Chem Res 2000;39(11):4040–53.
[20] Basu P, Mettanant V. Biomass Gasification in Supercritical Water – A Review. Int J Chem React Eng 2009;7. https://doi.org/10.2202/1542-6580.1919.
[21] Lee CS, Conradie AV, Lester E. Review of supercritical water gasification with lignocellulosic real biomass as the feedstocks: Process parameters, biomass composition, catalyst development, reactor design and its challenges. Chem Eng J 2021;415:128837.
[22] Ibrahim ABA, Akilli H. Supercritical water gasification of wastewater sludge for hydrogen production. Int J Hydrogen Energy 2019;44(21):10328–49.
[23] Xu ZR, Zhu W, Li M. Influence of moisture content on the direct gasification of dewatered sludge via supercritical water. Int J Hydrogen Energy 2012;37:6527–35. https://doi.org/10.1016/j.ijhydene.2012.01.086.
[24] Chen J, Liang J, Xu Z, E J. Assessment of supercritical water gasification process for combustible gas production from thermodynamic, environmental and techno-economic perspectives: A review. Energy Convers Manag 2020;226:113497.
[25] Cao W, Cao C, Guo L, Jin H, Dargusch M, Bernhardt D, et al. Hydrogen production from supercritical water gasification of chicken manure. Int J Hydrogen Energy 2016;41(48):22722–31.
[26] Onigbajumo A, Taghipour A, Will G, Chu Van T, Couperthwaite S, Steinberg T, et al. Effects of process-thermal configuration on energy, exergy, and thermo-economic performance of solar driven supercritical water gasification. Energy Convers Manag 2022;251:115002.
[27] Louw J, Schwarz CE, Knoetze JH, Burger AJ. Thermodynamic modelling of supercritical water gasification: Investigating the effect of biomass composition to aid in the selection of appropriate feedstock material. Bioresour Technol 2014;174:11–23.
[28] Rahbari A, Venkataraman MB, Pye J. Energy and exergy analysis of concentrated solar supercritical water gasification of algal biomass. Appl Energy 2018;228:1669–82.
[29] Okolie JA, Rana R, Nanda S, Dalai AK, Kozinski JA. Supercritical water gasification of biomass: A state-of-the-art review of process parameters, reaction mechanisms and catalysis. Sustain Energy Fuels 2019;3(3):578–98.
[30] Kruse A. Supercritical water gasification, Biofuels. Bioprod Biorefining 2008;2(5):415–37.

[31] Chen Z, Zhang X, Han W, Gao L, Li S. Exergy analysis on the process with integrated supercritical water gasification of coal and syngas separation. Appl Therm Eng 2018;128:1003–8.
[32] Darmawan A, Ajiwibowo MW, Cahyo FA, Aziz M, Tokimatsu K. Co-production of hydrogen and power from palm mill wastes, in. Energy Procedia 2019;158:1891–6.
[33] Guo S, Meng F, Peng P, Xu J, Jin H, Chen Y, et al. Thermodynamic analysis of the superiority of the direct mass transfer design in the supercritical water gasification system. Energy 2022;244:122722.
[34] Recalde M, Woudstra T, Aravind PV. Gasifier, Solid Oxide Fuel Cell Integrated Systems for Energy Production From Wet Biomass. Front Energy Res 2019;7. https://doi.org/10.3389/fenrg.2019.00129.
[35] Toonssen R, Aravind PV, Smit G, Woudstra N, Verkooijen AHM. System study on hydrothermal gasification combined with a hybrid solid oxide fuel cell gas turbine. Fuel Cells 2010;10(4):643–53.
[36] Facchinetti E, Gassner M, D'Amelio M, Marechal F, Favrat D. Process integration and optimization of a solid oxide fuel cell - Gas turbine hybrid cycle fueled with hydrothermally gasified waste biomass. Energy 2012;41(1):408–19.
[37] Chen Z, Gao L, Zhang X, Han W, Li S. High-efficiency power generation system with integrated supercritical water gasification of coal. Energy 2018;159:810–6.
[38] Samavati M, Santarelli M, Martin A, Nemanova V. Thermodynamic and economy analysis of solid oxide electrolyser system for syngas production. Energy 2017;122:37–49.
[39] Yakaboylu O, Harinck J, Gerton Smit KG, de Jong W. Supercritical water gasification of manure: A thermodynamic equilibrium modeling approach. Biomass Bioenergy 2013;59:253–63.
[40] Du Y, Qin Y, Zhang G, Yin Y, Jiao K, Du Q. Modelling of effect of pressure on co-electrolysis of water and carbon dioxide in solid oxide electrolysis cell. Int J Hydrogen Energy 2019;44(7):3456–69.
[41] Lo Faro M, Oliveira da Silva W, Valenzuela Barrientos W, Saglietti GGA, Zignani SC, Ticianelli EA, et al. The role of CuSn alloy in the co-electrolysis of CO2 and H2O through an intermediate temperature solid oxide electrolyser. J Energy Storage 2020;27:100820.
[42] Hauck M, Herrmann S, Spliethoff H. Simulation of a reversible SOFC with Aspen Plus. Int J Hydrogen Energy 2017;42:10329–40. https://doi.org/10.1016/j.ijhydene.2017.01.189.
[43] Libra JA, Ro KS, Kammann C, Funke A, Berge ND, Neubauer Y, et al. Hydrothermal carbonization of biomass residuals: A comparative review of the chemistry, processes and applications of wet and dry pyrolysis. Biofuels 2011;2(1):71–106.
[44] TNO, ECN Phyllis classification, Phyllis2. (2020).
[45] Yakaboylu O, Harinck J, Smit KG, de Jong W. Supercritical water gasification of biomass: A detailed process modeling analysis for a microalgae gasification process. Ind Eng Chem Res 2015;54(21):5550–62.
[46] Kruse A. Supercritical water gasification, Biofuels. Bioprod Biorefining 2008;2:415–37. https://doi.org/10.1002/bbb.93.
[47] Biswas S, Kulkarni AP, Fini D, Singh Rathore S, Seeber A, Giddey S, et al. Catalyst-induced enhancement of direct methane synthesis in solid oxide electrolyser. Electrochim Acta 2021;391:138934.
[48] Wendel CH, Kazempoor P, Braun RJ. A thermodynamic approach for selecting operating conditions in the design of reversible solid oxide cell energy systems. J Power Sources 2016;301:93–104. https://doi.org/10.1016/j.jpowsour.2015.09.093.
[49] O'Hayre R, Cha S-W, Colella W, Prinz FB. Chapter 2: Fuel Cell Thermodynamics. In: Fuel Cell Fundam. Hoboken, New Jersey: John Wiley & Sons Inc; 2016. https://doi.org/10.1002/9781119191766.ch2.
[50] Bagotsky VS. Fundamentals of Electrochemistry: Second Ed 2005. https://doi.org/10.1002/047174199X.
[51] Lang M, Bohn C, Henke M, Schiller G, Willich C, Hauler F. Understanding the Current-Voltage Behavior of High Temperature Solid Oxide Fuel Cell Stacks. J Electrochem Soc 2017;164(13):F1460–70.
[52] Zhu H, Kee RJ, Janardhanan VM, Deutschmann O, Goodwin DG. Modeling Elementary Heterogeneous Chemistry and Electrochemistry in Solid-Oxide Fuel Cells. J Electrochem Soc 2005;152:A2427. https://doi.org/10.1149/1.2116607.
[53] Wang S, Hao X, Zhan W. Research on a low temperature reversible solid oxide cell. Int J Hydrogen Energy 2017;42:29881–7. https://doi.org/10.1016/j.ijhydene.2017.09.181.
[54] Bernadet L, Laurencin J, Roux G, Montinaro D, Mauvy F, Reytier M. Effects of Pressure on High Temperature Steam and Carbon Dioxide Co-electrolysis. Electrochim Acta 2017;253:114–27. https://doi.org/10.1016/j.electacta.2017.09.037.
[55] Kazempoor P, Braun RJ. Model validation and performance analysis of regenerative solid oxide cells for energy storage applications: Reversible operation. Int J Hydrogen Energy 2014:5955–71. https://doi.org/10.1016/j.ijhydene.2014.01.186.
[56] M.J. Moran, Engineering thermodynamics: Fundamentals, in: I. John Wiley & Sons (Ed.), CRC Handb. Therm. Eng. Second Ed., Matthew Deans, United States of America, 2017. https://doi.org/10.4324/9781315119717.
[57] Nurdiawati A, Zaini IN, Irhamna AR, Sasongko D, Aziz M. Novel configuration of supercritical water gasification and chemical looping for highly-efficient hydrogen production from microalgae. Renew Sustain Energy Rev 2019;112:369–81.
[58] Botta G, Patel H, Sebastiani F, Aravind PV. Thermodynamic and Exergy Analysis of Reversible Solid Oxide Cell Systems. ECS Trans 2015;68:3265–77. https://doi.org/10.1017/CBO9781107415324.004.
[59] Fernandes A, Brabandt J, Posdziech O, Saadabadi A, Recalde M, Fan L, et al. Design, construction, and testing of a gasifier-specific solid oxide fuel cell system. Energies 2018;11(8):1985.
[60] Tanim T, Bayless DJ, Trembly JP. Modeling a 5 kWeplanar solid oxide fuel cell based system operating on JP-8 fuel and a comparison with tubular cell based system for auxiliary and mobile power applications. J Power Sources 2014;245:986–97. https://doi.org/10.1016/j.jpowsour.2013.07.008.
[61] Parks G, Boyd R, Cornish J, Remick R. Hydrogen Station Compression, Storage, and Dispensing Technical Status and Costs. Systems Integration 2014.
[62] Whiston MM, Collinge WO, Bilec MM, Schaefer LA. Exergy and economic comparison between kW-scale hybrid and stand-alone solid oxide fuel cell systems. J Power Sources 2017;353:152–66.
[63] Tabish AN, Patel HC, Schoonman J, Aravind PV. A detailed look into hydrogen electrochemical oxidation on ceria anodes. Electrochim Acta 2018;283:789–97.
[64] Banner J, Akter A, Wang R, Pietras J, Sulekar S, Marina OA, et al. Rare earth Nickelate electrodes containing heavily doped ceria for reversible solid oxide fuel cells. J Power Sources 2021;507:230248.
[65] Ioannidou E, Chavani M, Neophytides SG, Niakolas DK. Effect of the PH2O/PCO2 and PH2 on the intrinsic electro-catalytic interactions and the CO production pathway on Ni/GDC during solid oxide H2O/CO2 co-electrolysis. J Catal 2021;404:174–86.
[66] Wang L, Rao M, Diethelm S, Lin T-E, Zhang H, Hagen A, et al. Van herle, Power-to-methane via co-electrolysis of H2O and CO2: The effects of pressurized operation and internal methanation. Appl Energy 2019;250:1432–45.
[67] AlZahrani AA, Dincer I. Modeling and performance optimization of a solid oxide electrolysis system for hydrogen production. Appl Energy 2018;225:471–85.
[68] Oryshchyn D, Harun NF, Tucker D, Bryden KM, Shadle L. Fuel utilization effects on system efficiency in solid oxide fuel cell gas turbine hybrid systems. Appl Energy 2018;228:1953–65.
[69] Mastropasqua L, Pecenati I, Giostri A, Campanari S. Solar hydrogen production: Techno-economic analysis of a parabolic dish-supported high-temperature electrolysis system. Appl Energy 2020;261:114392.
[70] Reznicek EP, Braun RJ. Reversible solid oxide cell systems for integration with natural gas pipeline and carbon capture infrastructure for grid energy management. Appl Energy 2020;259:114118.
[71] Wang L, Zhang Y, Li C, Pérez-Fortes M, Lin T-E, Maréchal F, et al. Triple-mode grid-balancing plants via biomass gasification and reversible solid-oxide cell stack: Concept and thermodynamic performance. Appl Energy 2020;280:115987.
[72] Menon V, Janardhanan VM, Deutschmann O. A mathematical model to analyze solid oxide electrolyzer cells (SOECs) for hydrogen production. Chem Eng Sci 2014;110:83–93.